The present work was submitted to
Lehrstuhl für Mathematik (MathCCES)

Efficient Solvers for Computing the Scalar Magnetic Potential for Multiple Spheres

Master's Thesis
Computational Engineering Science

November 2017

Presented by	Christian Bauer christian.bauer@rwth-aachen.de
First examiner	Prof. Dr. Benjamin Stamm Lehrstuhl für Mathematik (MathCCES) RWTH Aachen University
Co-supervisor	Muhammad Hassan Lehrstuhl für Mathematik (MathCCES) RWTH Aachen University

Abstract. Since todays electronic devices are hitting a physical limit in terms of size and energy efficiency, it is vital to consider another basis for information processing and storage. The electron's spin state has a huge potential to overcome the aforementioned problems and is therefore studied in micromagnetic simulations. However, these simulations are time-consuming. Since the computation of the scalar magnetic potential (SMP) is the costliest part in terms of run time, in this Master's Thesis an efficient algorithm for computing the SMP of multiple spheres embedded in a cubic carrier material is presented. This setting, which in literature is known as a three-dimensional magnonic crystal, is described by a transmission problem. In order to solve it, we decouple the transmission problem into four different systems, two describing the cubic domain and two describing the spherical inclusions. The former two systems are then solved using a spectral collocation method and the single layer potential, respectively. For the latter two we exploit the properties of the spherical harmonics, construct a Galerkin method and introduce the fast multipole method (FMM) to efficiently handle multiple spheres. It is shown that the implemented methods display expected convergence and run time behavior. However, the collocation method has still potential for further improvements w.r.t. its run time and memory consumption. With this newly developed solver, the simulation of a three-dimensional magnonic crystal consisting of multiple spherical inclusions in a cubic carrier material might be accelerated, giving rise to more detailed spatial resolution or an extended physical time spans. For future research it would therefore be interesting to either extend the solver to a micromagnetic simulation framework or incorporate it into an existing simulation suite.

Zusammenfassung. Da die heutigen elektronischen Geräte in Bezug auf Größe und Energieeffizienz an physikalische Grenzen stoßen, ist es wichtig, eine neue Grundlage für die Informationsverarbeitung und -speicherung zu finden. Der Spinzustand des Elektrons hat ein enormes Potenzial, die oben genannten Probleme zu überwinden und wird daher in Mikromagnetismus-Simulationen untersucht. Diese Simulationen sind jedoch recht zeitaufwendig. Da die Berechnung des skalaren magnetischen Potenzials der kostenintensivste Teil der Laufzeit ist, wird in dieser Masterarbeit ein effizienter Algorithmus zur Berechnung des skalaren magnetischen Potenzials mehrerer Kugeln in einem kubischen Trägermaterial vorgestellt. Diese Struktur, die in der Literatur als dreidimensionaler Magnonic Crystal bekannt ist, wird durch ein Übergangsproblem beschrieben. Um es zu lösen, entkoppeln wir das Problem und erhalten so vier verschiedene Systeme, von denen zwei das kubische Gebiet und zwei die Vereinigungsmenge der sphärischen Gebiete beschreiben. Die beiden erstgenannten Systeme werden dann mit Hilfe einer spektralen Kollokationsmethode bzw. des Newton-Potenzials gelöst. Für die beiden letzteren nutzen wir die Eigenschaften der sphärischen, harmonischen Funktionen, konstruieren eine Galerkin-Methode und führen die Fast-Multipole-Methode ein, um mehrere Kugeln effizient berechnen zu können. Die implementierten Methoden zeigen ein erwartetes Konvergenz- und Laufzeitverhalten. Die Kollokationsmethode hat jedoch noch Potenzial für weitere Verbesserungen hinsichtlich der Laufzeit und des Speicherverbrauchs. Mit dem in dieser Arbeit neu entwickelten Löser könnte die Simulation eines dreidimensionalen Magnonic Crystals bestehend aus mehreren kugelförmigen Einschlüssen in einem kubischen Trägermaterial beschleunigt werden, um so eine detailliertere räumlichen Auflösung darstellen oder einen längeren physikalischen Zeitraum betrachten zu können. Als zukünftiges Forschungsthema wäre es daher interessant, den Algorithmus entweder zu einer Mikromagnetismus-Simulation zu erweitern oder in eine bestehende Simulations-Suite einzubinden.

Contents

List of Figures

List of Tables

1. Introduction

Todays electronic devices only exploit the electron's charge state. In current research the electron's spin is considered as another degree of freedom, allowing for a new category of data storages and data carriers: the spintronic devices. One group of these spintronic devices consists of magnonic information carriers and data storage devices. The term magnonic originates from the research topic of spin waves in nano-structure elements. A spin wave arises from the propagating reordering of magnetization in a material. The magnetization in turn arises from the electron's charge and spin state. In order to develop magnonic information carriers and data storage devices, magnonic crystals are studied. A magnonic crystal is a meta material with alternating magnetic properties that is made from geometric structuring. These crystals can enable magnonic band gaps allowing a selective propagation of spin waves through the material which would be the basis for magnonic logic devices. [25, 27]

Simulating such magnonic band gaps and magnonic crystals in general is done in micromagnetic simulations which essentially solve the Landau-Lifshitz-Gilbert (LLG) equation, an equation describing the magnetization's dynamic behavior [19]. The computationally most expensive part in these micromagnetic simulations is the computation of the scalar magnetic potential [7]. Therefore, solving for it efficiently is key. An efficient solver for the scalar magnetic potential for a unit sphere has already been developed in a previous seminar work [4]. Since a magnonic crystal would consist of many magnetic spheres in a cubic carrier material with different magnetic properties, the solver needs to be extended in order to simulate many spheres efficiently. In this Master's Thesis, the fast multipole method is therefore applied and incorporated into the existing code base.

In the following sections, the physical background of micromagnetic simulations is explained first — starting with a short quantum mechanical description of magnetism towards the famous Maxwell's equations and from the LLG equation towards the formulation of the scalar magnetic potential (SMP). Then, the mathematical description of the SMP's computation of a unit sphere is revisited and extended to many spheres. Afterwards, this formulation is discretized introducing the fast multipole method (FMM). The solvers for the four different subproblems are studied in detail and afterwards, the simulation results of the SMP of a magnonic crystal are presented. This Master's Thesis is then concluded with the results' discussion and an outlook into future research directions.

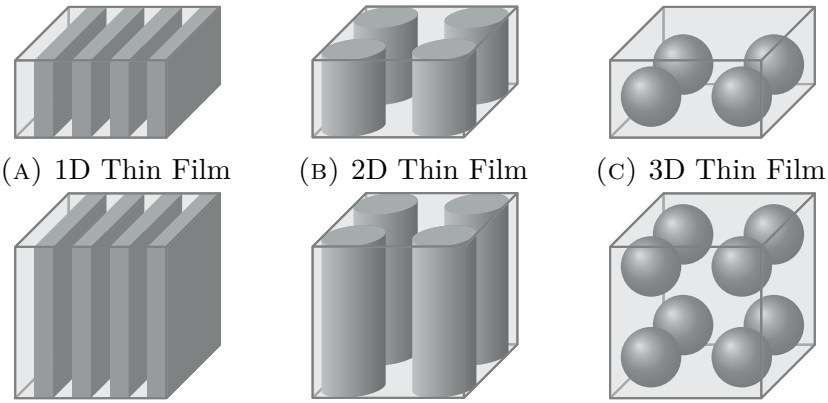

(a) 1D Thin Film (b) 2D Thin Film (c) 3D Thin Film

(d) 1D Bulk (e) 2D Bulk (f) 3D Bulk

Figure 1. The Different Types of Magnonic Crystals. In a thin film setting one spatial dimension is negligible compared to the other two spatial dimensions. The dimensions (1D, 2D, and 3D) refer to the periodicity of the different magnetic materials. So in the leftmost column the material only changes in one direction whereas in the rightmost column it changes in all three spatial dimensions. [Based on 16]

2. Physical Model

Magnonic crystals are magnetic metamaterials created by geometric structuring (see, e.g. Fig. 1). These structures are built out of small inclusions of a material with some magnetic properties in a matrix of another material with different magnetic properties. Through a periodic distribution of such inclusions the magnetic properties of a magnonic crystal are altered, consequentially controlling the spin wave (see Fig. 2) excitation as well as its propagation. In order to simulate this behavior the Landau-Lifshitz-Gilbert (LLG) equation is often used [1, 13]. Starting with a short introduction to the quantized view of magnetism it will be zoomed out to describe magnetism continuously. Afterwards, the LLG equation is introduced together with different energy terms that, when minimized, imply the material's magnetization $\vec{\mathbf{M}}$ in the steady-state.

2.1. Physical Preliminaries.

Henceforth, the following definitions are used.

Definition 2.1 (Magnetic Domain)**.** *Let $\Omega_{mag} \subset \mathbb{R}^3$ define a magnetic domain. Its boundary is then denoted as $\Gamma_{mag} \coloneqq \partial\Omega_{mag}$.*

Definition 2.2 (Free Space)**.** *The space not occupied by a magnetic domain Ω_{mag} is denoted as $\Omega_0 \coloneqq \mathbb{R}^3 \setminus \overline{\Omega_{mag}}$.*

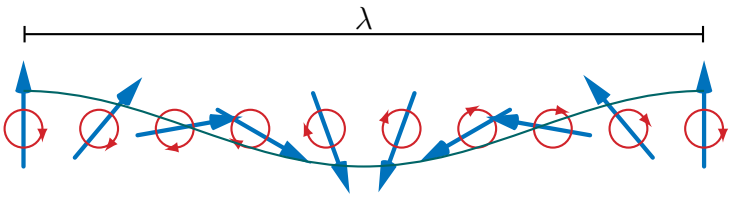

Figure 2. A Magnon Spin Wave. Through quantum mechanical effects, a magnon's movement affects its neighbors. This results in a wave-like reordering of magnons called the spin wave.

2.2. **Magnetization.** The fundamental nature of magnetism lies in the material's quantum mechanical properties. Observing an electron's position over a period yields different orbitals which then can be described by three, so called orbital integer quantum numbers (the principle quantum number n, the azimuthal quantum number ℓ, and the magnetic quantum number m). Together with the spin quantum number which parameterizes an electron's angular momentum, an electron in an atom is completely described. Both the three orbital quantum numbers and the spin quantum number are sources of magnetism, but for different types of magnets[1] some of them might be negligible. In a ferromagnetic material for example, the spin quantum number is the main source of magnetism [13] and therefore the magnetic dipole moment $\vec{\mathbf{m}}$, which can be thought of as a magnetic equivalent to an electron, can be expressed as

$$\vec{\mathbf{m}} \propto -\frac{e\vec{\mathbf{p}}_s}{m_e}. \tag{2.1}$$

Here, e and m_e denote the electron's charge and mass, respectively, and $\vec{\mathbf{p}}_s$ its spin state [7, 13]. These magnetic dipole moments (sometimes just called magnetic moments) are the quantized building blocks of magnetic matter.

The foundation of micromagnetic simulations is the continuous description of these quantized moments that form magnetism. This continuous description is called magnetization. It is a vector field $\vec{\mathbf{M}}(\vec{\mathbf{x}})\colon \mathbb{R}^3 \to \mathbb{R}^3$ that describes the density of magnetic moments inside a magnetic material, i.e.

$$\int_{\Omega_{\text{unit}}} \vec{\mathbf{M}}\, \mathrm{d}\Omega_{\text{unit}} = \vec{\mathbf{m}} \tag{2.2}$$

with $\vec{\mathbf{m}}$ being the magnetic moment and Ω_{unit} being the unit volume. This description only holds for volumes $\Omega_{\text{mag}} \geq \lambda^3$ where λ denotes the so called exchange interaction length (see Section 2.4.1), and therefore,

[1] There are different types of magnetism with ferromagnetism being the strongest and the commonly known one. Besides that there are paramagnetism, diamagnetism, and antiferromagnetism. Throughout this Thesis only ferromagnetic materials are considered, because of their importance in engineering applications, namely the magnetization's stability and the ability to create high magnetic induction fields [13].

such simulations are valid in length scales greater than or equal to 1 nm. Since the computation of the underlying equations is quite expensive the length scales nowadays have an upper limit of about 1000 nm. [1, 13]

2.3. **Landau-Lifshitz-Gilbert Equation.** In order to simulate spin waves in a ferromagnetic magnonic crystal, the evolution of the magnetization $\vec{\mathbf{M}}$ is of interest, which is described by the LLG equation. Let $\vec{\mathbf{M}}\colon \mathbb{R}^3 \to \mathbb{R}^3$, $\vec{\mathbf{H}}_{\text{eff}}\colon \mathbb{R}^3 \to \mathbb{R}^3$, and $\alpha, \gamma, M_{\text{s}} \in \mathbb{R}$. Then the LLG reads

$$\frac{\partial \vec{\mathbf{M}}}{\partial t} = -\gamma \left(\vec{\mathbf{M}} \times \vec{\mathbf{H}}_{\text{eff}}\right) - \frac{\alpha\gamma}{M_{\text{s}}} \vec{\mathbf{M}} \times \left(\vec{\mathbf{M}} \times \vec{\mathbf{H}}_{\text{eff}}\right). \tag{2.3}$$

Here, M_{s} describes the technical saturation magnetization (see Fig. 3) under an applied magnetic field, i.e.

$$\vec{\mathbf{m}}(\vec{\mathbf{x}}) = M_{\text{s}} \cdot \frac{\vec{\mathbf{m}}(\vec{\mathbf{x}})}{\|\vec{\mathbf{m}}(\vec{\mathbf{x}})\|}. \tag{2.4}$$

This technical saturation magnetization is reached when the magnetic moments in a material are aligned and are pointing in the same direction. In the literature the technical saturation magnetization is often referred to as the saturation magnetization. However, there is a slight difference between both terms (see Fig. 3). While the technical saturation in ferromagnetic materials is reached by applying a relatively weak magnetic field, the saturation can only be forced with a strong magnetic field. This is due to the thermal activation that causes misalignments in the magnetic moments. There are two dimensionless coefficients γ and α in Eq. (2.3) which describe the magnetization vector's change of orientation with respect to the direction of the effective magnetic field $\vec{\mathbf{H}}_{\text{eff}}$. The gyromagnetic ratio γ is a parameter that describes the magnetization's rotation around the direction of the effective field (see Fig. 4) and the damping coefficient α is a measure of the alignment of both fields. The effective magnetic field strength $\vec{\mathbf{H}}_{\text{eff}}\colon \mathbb{R}^3 \to \mathbb{R}^3$ is the resulting field after applying a magnetic field strength to the setting of interest, i.e.

$$\vec{\mathbf{H}}_{\text{eff}} = \vec{\mathbf{H}}_{\text{app}} + \vec{\mathbf{H}}_{\text{internal}}, \tag{2.5}$$

which is the sum of the applied magnetic field strength and the internal field strengths. [1, 3, 9, 13, 23]

In order to solve the LLG equation an initial condition is necessary. Such an initial condition for the magnetization $\vec{\mathbf{M}}$ is usually obtained by minimizing the total energy, i.e.

$$\begin{aligned} \vec{\mathbf{M}} &= \arg\min \left\{ E_{\text{Total}}\left(\vec{\mathbf{M}}'\right) \right\} \\ E_{\text{Total}}\left(\vec{\mathbf{M}}'\right) &= E_{\text{Exchange}} + E_{\text{Anisotropy}} + E_{\text{Zeeman}} + E_{\text{Demagnetization}}, \end{aligned} \tag{2.6}$$

which translates to the assumption that the system is in steady-state.

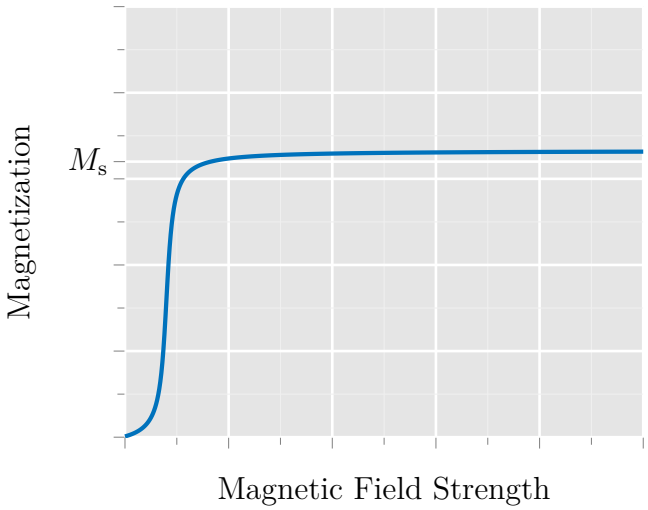

Figure 3. Technical Saturation Magnetization. After reaching the technical saturation, the magnetization increases only slowly while increasing $\vec{\mathbf{H}}$. This is due to thermal activation which slightly distorts the parallel alignment of neighboring magnons.

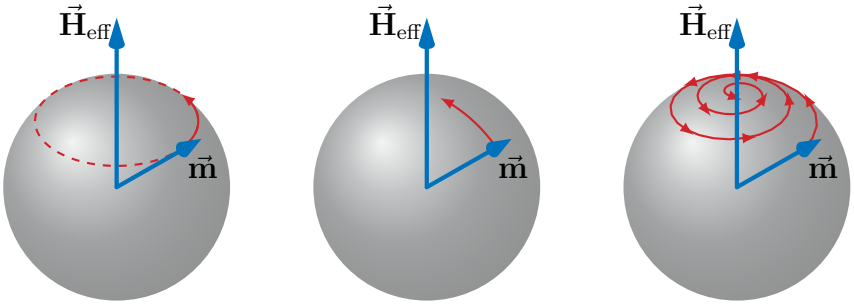

Figure 4. Precessional Motion Around the Effective Field with Damping. The magnetization $\vec{\mathbf{M}}$ rotates around the effective field $\vec{\mathbf{H}}_{\text{eff}}$, as described with the coefficient γ (left), and the damping α (middle) results in a spiralling motion (right). [Based on 1]

2.4. **Magnetic Interaction Energies.** The different interaction energies in Eq. (2.6) are now explained. Note that depending on the type of simulation some terms can be neglected, if their impact is small enough. [See, e.g., 1, 7, 9, 12].

2.4.1. *Exchange Energy.* The exchange energy is responsible for the spontaneous magnetization of a body. It is based on the Coulomb interaction as well as the quantum mechanical Pauli exclusion principle and energetically favors a parallel alignment of neighboring spins. The

continuous description of the exchange energy reads

$$E_{\text{Exchange}} = \frac{A_{\text{ex}}}{V} \int_{\Omega_{\text{mag}}} \left(\boldsymbol{\nabla} \cdot \vec{\mathbf{M}}\right)^2 \mathrm{d}\Omega_{\text{mag}} \,, \tag{2.7}$$

with a measure for the exchange stiffness denoted A_{ex} and the magnet's volume V. Although the exchange energy has limited range, its magnitude causes spontaneous long-range ordering in ferromagnets. [12]

2.4.2. *Anisotropic Energy.* The anisotropy energy results from spin-orbit interactions. It describes the alignment of a magnetization parallel to certain axes depending on the material's lattice structure. These axes are called easy axes. For a magnet with only one easy axis, the anisotropy energy is defined by

$$E_{\text{Anisotropy}} = K_{u1} \int_{\Omega_{\text{mag}}} \sin^2(\varphi)\, \mathrm{d}\Omega_{\text{mag}} + K_{u2} \int_{\Omega_{\text{mag}}} \sin^4(\varphi)\, \mathrm{d}\Omega_{\text{mag}} \,. \tag{2.8}$$

Here, K_{u1} and K_{u2} are the uni-axial anisotropy constants and φ is the angle between the magnetization vector $\vec{\mathbf{M}}$ and the easy axis. [See, e.g., 1, 7, 13]

2.4.3. *Zeeman Energy.* Interactions with an applied magnetic field $\vec{\mathbf{H}}_{\text{app}}$ are described by the Zeeman energy

$$E_{\text{Zeeman}} = -\mu_0 \int_{\Omega_{\text{mag}}} \vec{\mathbf{M}} \cdot \vec{\mathbf{H}}_{\text{app}}\, \mathrm{d}\Omega_{\text{mag}} \tag{2.9}$$

which is minimized, if the magnetization is parallel to the external field. [1, 7, 12, 13]

2.4.4. *Demagnetization Energy.* The demagnetization energy accounts for the electrons' dipole-dipole interactions. In its continuous description the demagnetization energy reads

$$E_{\text{Demagnetization}} = -\frac{\mu_0}{2V} \int_{\Omega_{\text{mag}}} \vec{\mathbf{M}} \cdot \vec{\mathbf{H}}_{\text{demag}}\, \mathrm{d}\Omega_{\text{mag}} \,. \tag{2.10}$$

Here, the demagnetization field $\vec{\mathbf{H}}_{\text{demag}}$, also referred to as stray field, is introduced. The stray field energy describes a long-ranged interaction in which the demagnetization, that is induced by the magnetization itself, counteracts the magnetization. Calculating the stray field is one of the most important steps in evaluating the effective field, because the demagnetization field often dominates the other fields. [1, 12, 14]

2.5. **Demagnetization Field.** In this Thesis, the focus is on the computation of the demagnetization energy or field, because of its physical importance [13] and computational cost (see Fig. 5). The demagnetization field can be derived from Maxwell's equations which describe electromagnetism in general.

The following derivation is mainly drawn from Feynman, Leighton, and Sands [8] and Jiles [13]. Maxwell's laws of electromagnetism read

$$\boldsymbol{\nabla} \cdot \vec{\mathbf{E}} = \frac{\rho}{\epsilon_0} \tag{2.11a}$$

$$\boldsymbol{\nabla} \times \vec{\mathbf{E}} = -\frac{\partial \vec{\mathbf{B}}}{\partial t} \tag{2.11b}$$

$$\boldsymbol{\nabla} \times \vec{\mathbf{B}} = \mu_0 \left(\epsilon_0 \frac{\partial \vec{\mathbf{E}}}{\partial t} + \vec{\mathbf{J}} \right) \tag{2.11c}$$

$$\boldsymbol{\nabla} \cdot \vec{\mathbf{B}} = 0. \tag{2.11d}$$

Here, the electric field $\vec{\mathbf{E}}$ and the magnetic induction $\vec{\mathbf{B}}$ as well as their interactions are modeled. The Eq. (2.11a) states that the electric flux through a closed surface $\boldsymbol{\nabla} \cdot \vec{\mathbf{E}}$ is proportional to the charge density ρ inside the volume. ϵ_0 is a physical constant called the permittivity of vacuum and measures the capability of vacuum to store electrical energy in an electric field. In the Eq. (2.11b) the negative rate of change of the magnetic flux $\frac{\partial \vec{\mathbf{B}}}{\partial t}$ enclosed by a loop is proportional to the induced voltage in the loop $\boldsymbol{\nabla} \times \vec{\mathbf{E}}$. In the Eq. (2.11c) the magnetic field induced around a closed loop $\boldsymbol{\nabla} \times \vec{\mathbf{B}}$ is proportional to the electric current $\vec{\mathbf{J}}$ plus the rate of change of the electric field that the loop encloses $\frac{\partial \vec{\mathbf{E}}}{\partial t}$. Finally, the Eq. (2.11d) states that the magnetic flux through a closed surface $\boldsymbol{\nabla} \cdot \vec{\mathbf{B}}$ is zero, therefore forbidding magnetic monopoles. The Eqs. (2.11a)–(2.11d) are referred to as Gauß's law, Faraday's law of induction, Ampère's circuital law, and Gauß's law for magnetism, respectively.

Assuming steady-state, the terms $\frac{\partial}{\partial t}(\cdot)$ vanish and therefore, the static system reads

$$\boldsymbol{\nabla} \cdot \vec{\mathbf{E}} = \frac{\rho}{\epsilon_0} \tag{2.12a}$$

$$\boldsymbol{\nabla} \times \vec{\mathbf{E}} = 0 \tag{2.12b}$$

$$\boldsymbol{\nabla} \times \vec{\mathbf{B}} = \mu_0 \vec{\mathbf{J}} \tag{2.12c}$$

$$\boldsymbol{\nabla} \cdot \vec{\mathbf{B}} = 0. \tag{2.12d}$$

In contrast to Eq. (2.11) the equations for the electric and magnetic fields are decoupled. Therefore, the equations containing the electric field $\vec{\mathbf{E}}$ are therefore dropped.

The magnetic induction is not the only field that is used to describe a material's magnetic properties. In the literature another field is often used to describe magnetism: the magnetic field strength $\vec{\mathbf{H}}$ which relates

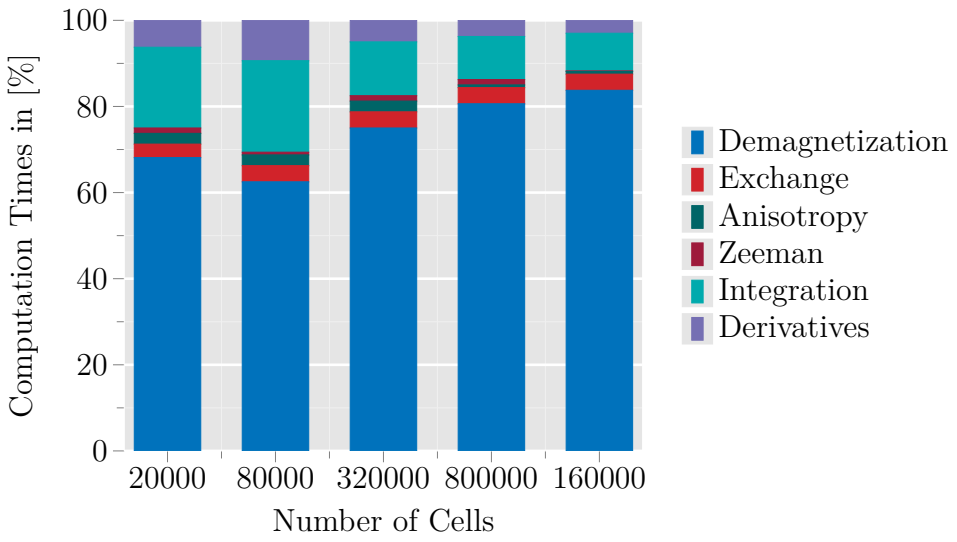

Figure 5. Time Spent for Different Computations in a Micromagnetic Simulation over Number of Cells. [Based on 7]

to the magnetic induction field in the following way

$$\vec{\mathbf{H}} = \begin{cases} \dfrac{\vec{\mathbf{B}}}{\mu_0}, & \text{in} \quad \Omega_0 \\ \vec{\mathbf{H}} = \dfrac{\vec{\mathbf{B}}}{\mu_0} - \vec{\mathbf{M}}, & \text{in} \quad \Omega_{\text{mag}}. \end{cases} \tag{2.13}$$

Now the demagnetization field is derived. This field is defined as the magnetic field strength $\vec{\mathbf{H}}_{\text{dem}} \colon \mathbb{R}^3 \to \mathbb{R}^3$ generated by the magnetization $\vec{\mathbf{M}}$ of a magnet occupying the domain $\Omega_{\text{mag}} \subset \mathbb{R}^3$. Additionally, the absence of free currents, i.e. $\vec{\mathbf{J}} = 0$, is assumed[2]. Ampère's law in a magnetostatic system then reads

$$\boldsymbol{\nabla} \times \vec{\mathbf{H}}_{\text{dem}} = 0. \tag{2.14}$$

2.6. **Scalar Magnetic Potential.** From Eq. (2.14) we know that $\vec{\mathbf{H}}_{\text{dem}}$ is a curl-free vector field and can be described by a scalar potential $\phi \colon \mathbb{R}^3 \to \mathbb{R}$, i.e.

$$\vec{\mathbf{H}}_{\text{dem}} = -\boldsymbol{\nabla}\phi. \tag{2.15}$$

[2]The assumption of no free currents is actually not necessary (see Langer [17]), but would result in a more complicated derivation. However, the presented results can be extended to also handle free currents.

In this case the potential is called *scalar magnetic potential*. Let $\chi_{\Omega_{\text{mag}}}$ be a characteristic function [1], s.t.

$$\chi_{\Omega_{\text{mag}}} = \begin{cases} 1, & \text{in} \quad \Omega_{\text{mag}} \\ 0, & \text{in} \quad \Omega_0. \end{cases} \tag{2.16}$$

Inserting Eq. (2.13) into Gauß's law for magnetism and using the characteristic function results in

$$\Delta\phi = \boldsymbol{\nabla} \cdot \left(\vec{\mathbf{M}}\chi_{\Omega_{\text{mag}}}\right). \tag{2.17}$$

We now need to define the notation of the jump as well as the normal derivative.

Definition 2.3 (Jump)**.** *Consider two domains that share a common boundary. We denote them by Ω_1 and Ω_2. Let u be a scalar defined over both domains and write u_1 (resp. u_2) to evaluate u from within the domain Ω_1 (Ω_2), i.e. $u_i = u|_{\Omega_i}, \quad i = \{1, 2\}$. Let $\vec{\mathbf{n}}_1$ and $\vec{\mathbf{n}}_2$ be the outward pointing unit normals of domain 1 and 2, respectively. For a scalar, we define the jump over the shared boundary as*

$$[u] \coloneqq u_1 \cdot \vec{\mathbf{n}}_1 + u_2 \cdot \vec{\mathbf{n}}_2. \tag{2.18}$$

Let now $\vec{\mathbf{v}}$ be a vector defined on Ω_1 and Ω_2. We define the jump over the shared boundary as

$$[\vec{\mathbf{v}}] \coloneqq \vec{\mathbf{v}}_1 \cdot \vec{\mathbf{n}}_1 + \vec{\mathbf{v}}_2 \cdot \vec{\mathbf{n}}_2. \tag{2.19}$$

Definition 2.4 (Normal Derivative)**.** *Let $\vec{\mathbf{n}}$ be an outward pointing unit normal of an arbitrary domain Ω. Additionally, let $u\colon \mathbb{R}^3 \to \mathbb{R}$ with $u \in C^1(\Omega)$ be a continuous function. We denote by*

$$\partial_{\vec{\mathbf{n}}} \coloneqq \boldsymbol{\nabla} u \cdot \vec{\mathbf{n}} \tag{2.20}$$

the normal derivative.

Transforming Eq. (2.17) into

$$\boldsymbol{\nabla} \cdot \left(\boldsymbol{\nabla}\phi - \vec{\mathbf{M}}\chi_{\Omega_{\text{mag}}}\right) = 0 \tag{2.21}$$

and using the definitions for the jumps, one can show that ϕ satisfies

$$\begin{aligned} [\partial_{\vec{\mathbf{n}}}\phi] &= \left[\vec{\mathbf{M}}\right], \quad \text{on} \quad \Gamma_{\text{mag}} \\ [\phi] &= 0, \qquad \text{on} \quad \Gamma_{\text{mag}}. \end{aligned} \tag{2.22}$$

Physically, this means that the potential ϕ as well as the normal flux $\left(\boldsymbol{\nabla}\phi - \vec{\mathbf{M}}\right) \cdot \vec{\mathbf{n}}$ across the boundary should be continuous [24]. With $\left[\vec{\mathbf{M}}\chi_{\Omega_{\text{mag}}}\right] = -\vec{\mathbf{M}} \cdot \vec{\mathbf{n}}$, where $\vec{\mathbf{n}}$ is the outward pointing unit normal, we

get

$$
\begin{aligned}
\Delta\phi &= \boldsymbol{\nabla}\cdot\left(\vec{\mathbf{M}}\right) && \text{in} && \Omega_{\text{mag}} \\
\Delta\phi &= 0 && \text{in} && \Omega_0 \\
[\partial_{\vec{\mathbf{n}}}\phi] &= -\vec{\mathbf{M}}\cdot\vec{\mathbf{n}} && \text{on} && \Gamma_{\text{mag}} \\
[\phi] &= 0 && \text{on} && \Gamma_{\text{mag}},
\end{aligned}
\tag{2.23}
$$

which in mathematical literature is referred to as a transmission problem [see, e.g., 24].

2.7. **Geometric Setup for a Magnonic Crystal.** In this Thesis we study a magnonic crystal which is built from two different magnetic materials denoted by the subscripts 1 and 2, respectively. It is assumed that the magnonic crystal consists of a cubic carrier material with spherical inclusions (see Fig. 6). In addition to the free space we define the following two domains.

Definition 2.5 (Spherical Domain)**.** *For N spheres we define a domain Ω_1 as*

$$\Omega_1 \coloneqq \bigcup_{i=1}^{N} B_{r_i}(\vec{\mathbf{c}}_i).$$

Here, r_i denotes the i-th sphere's radius and $\vec{\mathbf{c}}_i$ its center.

Definition 2.6 (Cubic Domain)**.** *Let $P \in \mathbb{R}^3$ denote a rectangular prism in three dimensions. Then, Ω_2 is defined as*

$$\Omega_2 \coloneqq P \setminus \Omega_1.$$

Additionally, we define two boundaries.

Definition 2.7 (Boundaries)**.** *Let the spheres' boundary be*

$$\Gamma_1 \coloneqq \partial\Omega_1.$$

Then, the cuboid's outer boundary (which does not include the spheres' boundary) is defined as

$$\Gamma_2 \coloneqq \partial\Omega_2 \setminus \Gamma_1.$$

Remark. *The corresponding magnetizations are denoted by $\vec{\mathbf{M}}_1 \coloneqq \vec{\mathbf{M}}|_{\Omega_1}$ and $\vec{\mathbf{M}}_2 \coloneqq \vec{\mathbf{M}}|_{\Omega_2}$.*

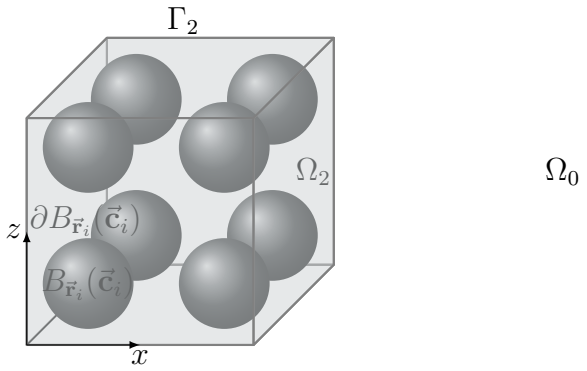

Figure 6. A Magnonic Crystal. The crystal consists of $N = 8$ spherical inclusions Ω_1 with boundary Γ_1 embedded in a cubic carrier material Ω_2 with boundary Γ_2. The free space is denoted by Ω_0.

With these definitions we have $\Omega_{\text{mag}} = \Omega_1 \cup \Omega_2$ and therefore, we obtain from Eq. (2.17) the transmission problem

$$
\begin{aligned}
\Delta\phi &= \boldsymbol{\nabla} \cdot \vec{\mathbf{M}}_1 && \text{in} \quad \Omega_1 \\
\Delta\phi &= \boldsymbol{\nabla} \cdot \vec{\mathbf{M}}_2 && \text{in} \quad \Omega_2 \\
\Delta\phi &= 0 && \text{in} \quad \Omega_0 \\
[\phi] &= 0 && \text{on} \quad \Gamma_1 \cup \Gamma_2 \\
[\partial_{\vec{\mathbf{n}}}\phi] &= -(\vec{\mathbf{M}}_1 - \vec{\mathbf{M}}_2) \cdot \vec{\mathbf{n}} && \text{on} \quad \Gamma_1 \\
[\partial_{\vec{\mathbf{n}}}\phi] &= -\vec{\mathbf{M}}_2 \cdot \vec{\mathbf{n}} && \text{on} \quad \Gamma_2.
\end{aligned}
\tag{2.24}
$$

After describing the physical setup that is studied in this Thesis, the following section will decouple Eq. (2.24) first and afterwards discuss the solvability of the obtained equations.

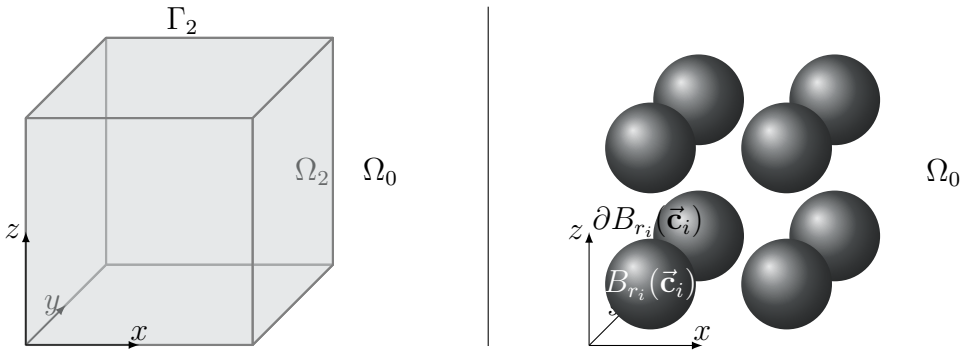

FIGURE 7. The Mathematical Splitting. The picture on the left corresponds to Eq. (3.1) and the one on the right to Eq. (3.2).

3. Mathematical Model

Starting with Eq. (2.24) a simplification in the strong formulation is derived first. Afterwards, the results are presented in their weak formulation and the problems' well-posedness is stated.

3.1. **Strong Formulation.** We now simplify Eq. (2.24) in the strong formulation. For this purpose the magnonic crystal is split into a cubic domain and a domain consisting of the spheres. In return, we get two similar systems which are split again. Finally, four systems that describe the magnonic crystal given in Eq. (2.24) are obtained.

For the cubic domain $\Omega_1 \cup \Omega_2$, let $v\colon \mathbb{R}^3 \to \mathbb{R}$ be defined as the solution to the transmission problem

$$\begin{aligned} \Delta v &= \boldsymbol{\nabla} \cdot \left(\vec{\mathbf{M}}_2\right) && \text{in} \quad \Omega_1 \cup \Omega_2 \\ \Delta v &= 0 && \text{in} \quad \Omega_0 \\ [v] &= 0 && \text{on} \quad \Gamma_2 \\ [\partial_{\vec{\mathbf{n}}} v] &= -(\vec{\mathbf{M}}_2 \cdot \vec{n}) && \text{on} \quad \Gamma_2. \end{aligned} \tag{3.1}$$

For the spherical domain Ω_1, we define $u\colon \mathbb{R}^3 \to \mathbb{R}$ to be the solution to

$$\begin{aligned} \Delta u &= \boldsymbol{\nabla} \cdot \left(\vec{\mathbf{M}}_1 - \vec{\mathbf{M}}_2\right) && \text{in} \quad \Omega_1 \\ \Delta u &= 0 && \text{in} \quad \Omega_0 \cup \Omega_2 \\ [u] &= 0 && \text{on} \quad \Gamma_1 \\ [\partial_{\vec{n}} u] &= -((\vec{\mathbf{M}}_1 - \vec{\mathbf{M}}_2) \cdot \vec{n}) && \text{on} \quad \Gamma_1, \end{aligned} \tag{3.2}$$

and state the following lemma.

Lemma 3.1. *Solving the Eqs.* (3.1) *and* (3.2) *yields the solution to Eq.* (2.24)*, i.e.*

$$\phi = u + v.$$

Proof. Indeed, inserting this solution into Eq. (2.24) and using the linearity of the Laplacian and the divergence yields

$$\Delta\phi = \Delta u + \Delta v = \boldsymbol{\nabla} \cdot \vec{\mathbf{M}}_1 \quad \text{in} \quad \Omega_1. \quad \checkmark$$

Similarly, for the domains Ω_2 and Ω_0, inserting $u + v$ yields

$$\begin{aligned} \Delta\phi = \Delta u + \Delta v = \boldsymbol{\nabla} \cdot \vec{\mathbf{M}}_2 \quad &\text{in} \quad \Omega_2 \quad \checkmark \\ \Delta\phi = \Delta u + \Delta v = 0 \quad &\text{in} \quad \Omega_0 \quad \checkmark. \end{aligned}$$

It remains to show equivalence for the jump conditions. Since the transmission is linear, too, inserting the corresponding subproblem's solution results in

$$[\phi] = [u + v] = [u] + [v] = 0 \quad \text{on} \quad \Gamma_2 \cup \Gamma_1 \quad \checkmark$$

as well as

$$[\partial_{\vec{\mathbf{n}}}\phi] = [\partial_{\vec{\mathbf{n}}}u] + [\partial_{\vec{\mathbf{n}}}v] \quad \text{on} \quad \Gamma_1$$

and since the solution to the Laplace equation in $\Omega_2 \cup \Omega_1$ has no discontinuities across Γ_1, i.e. $[\partial_{\vec{\mathbf{n}}}v = 0]$

$$[\partial_{\vec{\mathbf{n}}}\phi] = -((\vec{\mathbf{M}}_1 - \vec{\mathbf{M}}_2) \cdot \vec{n}) \quad \text{on} \quad \Gamma_1. \quad \checkmark$$

Similarly, on the boundary Γ_2 the transmission condition is

$$[\partial_{\vec{\mathbf{n}}}\phi] = [\partial_{\vec{\mathbf{n}}}u] + [\partial_{\vec{\mathbf{n}}}v] = -\vec{\mathbf{M}}_2 \cdot \vec{n} \quad \text{on} \quad \Gamma_2. \quad \checkmark$$

□

We emphasize the structural equivalence of the two transmission problems Eqs. (3.1) and (3.2), formulate an abstract version of this type of system, and introduce another decoupling.

Let $w\colon \mathbb{R}^3 \to \mathbb{R}$, $f\colon \mathbb{R}^3 \to \mathbb{R}$, and $g\colon \mathbb{R}^3 \to \mathbb{R}$. The abstraction to Eqs. (3.1) and (3.2) reads

$$\begin{aligned} \Delta w &= f \quad \text{in} \quad \Omega_{\text{mag}} \\ \Delta w &= 0 \quad \text{in} \quad \Omega_0 \\ [w] &= 0 \quad \text{on} \quad \Gamma_{\text{mag}} \\ [\partial_{\vec{\mathbf{n}}} w] &= g \quad \text{on} \quad \Gamma_{\text{mag}}. \end{aligned} \tag{3.3}$$

Remark. *Setting $\Omega_{mag} = \Omega_1 \cup \Omega_2$ or $\Omega_{mag} = \Omega_1$ and Γ as well as f and g accordingly, results in Eq.* (3.1) *or Eq.* (3.2)*.*

Let $w_{\text{int}}\colon \mathbb{R}^3 \to \mathbb{R}$ be the solution to the interior problem

$$\begin{aligned} \Delta w_{\text{int}} &= f \quad \text{in} \quad \Omega_{\text{mag}} \\ w_{\text{int}} &= 0 \quad \text{on} \quad \Gamma_{\text{mag}}. \end{aligned} \tag{3.4}$$

In literature, this problem is known as an interior Dirichlet problem [see, e.g., 24]. With this system and with $w_{\text{ext}}\colon \mathbb{R}^3 \to \mathbb{R}$ defined by the

solution of the following transmission problem

$$\begin{aligned} \Delta w_{\text{ext}} &= 0 && \text{in} \quad \mathbb{R}^3 \setminus \Gamma_{\text{mag}} \\ [w_{\text{ext}}] &= 0 && \text{on} \quad \Gamma_{\text{mag}} \\ [\partial_{\vec{\mathbf{n}}} w_{\text{ext}}] &= g - \partial_{\vec{\mathbf{n}}} w_{\text{int}}\Big|_{\Omega_{\text{mag}}} && \text{on} \quad \Gamma_{\text{mag}}, \end{aligned} \tag{3.5}$$

we can recover $w = w_{\text{int}} + w_{\text{ext}}$ as shown in the next lemma.

Lemma 3.2. *Solving Eqs.* (3.4) *and* (3.5) *yields the solution to Eq.* (3.3)*, i.e.*

$$w = w_{\text{int}} + w_{\text{ext}}.$$

Proof.

$$\begin{aligned} \Delta w = \Delta(w_{\text{int}} + w_{\text{ext}}) &= f && \text{in} \quad \Omega_{\text{mag}} \quad \checkmark \\ \Delta w = \Delta(w_{\text{int}} + w_{\text{ext}}) &= 0 && \text{in} \quad \Omega_0 \quad \checkmark \\ [w] = [w_{\text{int}}] + [w_{\text{ext}}] &= 0 && \text{on} \quad \Gamma_{\text{mag}} \quad \checkmark \\ [\partial_{\vec{n}} w] = [\partial_{\vec{n}} w_{\text{int}}] + [\partial_{\vec{n}} w_{\text{ext}}] &= g && \text{on} \quad \Gamma_{\text{mag}} \quad \checkmark \end{aligned}$$

□

For the Eq. (3.1) we now define $f\colon \mathbb{R}^3 \to \mathbb{R}$ by

$$f(\vec{\mathbf{x}}) = \boldsymbol{\nabla} \cdot \vec{\mathbf{M}}_2(\vec{\mathbf{x}})$$

and $g\colon \mathbb{R}^3 \to \mathbb{R}$ by

$$g(\vec{\mathbf{x}}) = -\vec{\mathbf{M}}_2(\vec{\mathbf{x}}) \cdot \vec{\mathbf{n}}(\vec{\mathbf{x}}).$$

Therefore, Eq. (3.1) is separated into an interior Dirichlet problem reading

$$\begin{aligned} \Delta v_{\text{int}} &= \boldsymbol{\nabla} \cdot \left(\vec{\mathbf{M}}_2\right), && \text{in} \quad \Omega_2 \\ v_{\text{int}} &= 0, && \text{on} \quad \Gamma_2 \end{aligned} \tag{3.6}$$

and a transmission problem reading

$$\begin{aligned} \Delta v_{\text{ext}} &= 0, && \text{in} \quad \mathbb{R}^3 \setminus \Gamma_2 \\ [v_{\text{ext}}] &= 0, && \text{on} \quad \Gamma_2 \\ [\partial_{\vec{\mathbf{n}}} v_{\text{ext}}] &= -\left(\vec{\mathbf{M}}_2 \cdot \vec{n}\right) - \partial_{\vec{n}} v_{\text{int}}\Big|_{\Omega_2}, && \text{on} \quad \Gamma_2. \end{aligned} \tag{3.7}$$

For the Eq. (3.2) we define $f\colon \mathbb{R}^3 \to \mathbb{R}$ by

$$f(\vec{\mathbf{x}}) = \boldsymbol{\nabla} \cdot \left(\vec{\mathbf{M}}_1(\vec{\mathbf{x}}) - \vec{\mathbf{M}}_2(\vec{\mathbf{x}})\right)$$

and $g\colon \mathbb{R}^3 \to \mathbb{R}$ by

$$g(\vec{\mathbf{x}}) = -\left(\vec{\mathbf{M}}_1(\vec{\mathbf{x}}) - \vec{\mathbf{M}}_2(\vec{\mathbf{x}})\right) \cdot \vec{\mathbf{n}}(\vec{\mathbf{x}}),$$

respectively. Therefore, we obtain an interior Dirichlet problem

$$\begin{aligned} \Delta u_{\text{int}} &= \boldsymbol{\nabla} \cdot \left(\vec{\mathbf{M}}_1 - \vec{\mathbf{M}}_2\right) && \text{in} \quad \Omega_1 \\ u_{\text{int}} &= 0 && \text{on} \quad \Gamma_1 \end{aligned} \tag{3.8}$$

and a transmission problem

$$\begin{aligned} \Delta u_{\text{ext}} &= 0 && \text{in} \quad \mathbb{R}^3 \setminus \Gamma_1 \\ [u_{\text{ext}}] &= 0 && \text{on} \quad \Gamma_1 \\ [\partial_{\vec{n}} u_{\text{ext}}] &= -(\vec{\mathbf{M}}_1 - \vec{\mathbf{M}}_2) \cdot \vec{n} - \partial_{\vec{n}} u_{\text{int}}|_{\Omega_1} && \text{on} \quad \Gamma_1. \end{aligned} \tag{3.9}$$

With Eqs. (3.6)–(3.9) we have formulated four systems of equations that are equivalent to the initial set of equations, i.e. Eq. (2.24). The motivation is that each of them can be discretized differently by taking advantage of the geometric properties. In the following section, the weak formulation for these systems is derived.

3.2. **Weak Formulation.** Now, the weak formulation for the two abstract problems Eqs. (3.4) and (3.5) is derived. In order to do this, the following mathematical tools are needed.

3.2.1. *Mathematical Preliminaries.*

Definition 3.1. *Let $u \in C^0(\Omega)$ be a continuous function inside the domain Ω. The support of u is defined as* $\operatorname{supp}(u) \coloneqq \overline{\{x \in \Omega \colon u(x) \neq 0\}}$. *Additionally, let C^∞ denote the space of infinitely differentiable functions. Then*

$$C_0^\infty(\Omega) \coloneqq \{u \in C^\infty(\Omega) \colon \operatorname{supp}(u) \subset\subset \Omega\} \tag{3.10}$$

is the space of infinitely continuous differentiable functions that have compact support on Ω, [see e.g., 24].

Definition 3.2. *The space of infinitely differentiable functions with compact support in $\mathbb{R}^3$ is defined as*

$$C_{comp}^\infty(\Omega) \coloneqq C_0^\infty\left(\mathbb{R}^3\right)\Big|_\Omega \coloneqq \left\{u\Big|_\Omega \colon u \in C_0^\infty\left(\mathbb{R}^3\right)\right\}. \tag{3.11}$$

Remark. *For $\Omega = \mathbb{R}^3$, the spaces C_{comp}^∞ and C_0^∞ are equal [24].*

Definition 3.3 (Sobolev Space [24])**.** *Let Ω be a domain. Then,*

$$H^s(\Omega) = \left\{f \in L^2(\Omega) \colon \partial^\alpha f \in L^2(\Omega), \forall |\alpha| \leq s\right\} \tag{3.12}$$

denotes the Sobolev space of order s on Ω.

Remark. *Let Ω be a domain with boundary Γ. The Sobolev space of functions that vanish on the boundary is defined as*

$$H_0^s(\Omega) = \left\{f \in L^2(\Omega) \colon \partial^\alpha f \in L^2(\Omega), \forall |\alpha| \leq s \wedge f\Big|_\Gamma = 0\right\} \tag{3.13}$$

Definition 3.4 (Dual of a Sobolev Space)**.** *Let Ω be a domain or boundary. The dual space of a Sobolev space $H_0^\ell(\Omega)$ is defined as*

$$H^{-\ell}(\Omega) \coloneqq \left(H_0^\ell(\Omega)\right)', \ell \geq 0, \tag{3.14}$$

[see, e.g., 24] and contains all bounded, linear functionals.

Definition 3.5. *Let Ω be a (possibly unbounded) domain. Then,*

$$H^{\ell}_{loc}(\Omega) \coloneqq \left\{u \in C^{\infty}_{comp}(\Omega)' \colon \nu u \in H^{\ell}(\Omega), \quad \forall \nu \in C^{\infty}_{comp}(\Omega)\right\} \tag{3.15}$$

is the space that contains all continuous, linear functionals (distributions)[24].

Remark. *For a bounded domain Ω the spaces $H^{\ell}_{loc}(\Omega)$ and $H^{\ell}(\Omega)$ coincide [24].*

Definition 3.6. *For transmission problems a suitable decay condition needs to be incorporated into the Sobolev space [24]. Let the scalar inner product for functions $u, v \in C^{\infty}_{comp}(\Omega)$ be defined as*

$$(u,v)_{H^1(\Delta,\Omega)} \coloneqq \int_{\Omega} \left(\langle \boldsymbol{\nabla} u, \boldsymbol{\nabla} \bar{v} \rangle + \frac{u\bar{v}}{1 + \|\vec{\mathbf{x}}\|^2} \right) \mathrm{d}\vec{\mathbf{x}}\,. \tag{3.16}$$

The spaces $C^{\infty}_{comp}(\Omega)$ and $C^{\infty}_{0}(\Omega)$ can be closed w.r.t. the norm

$$\|u\|_{H^1(\Delta,\Omega)} \coloneqq \sqrt{(u,u)} \tag{3.17}$$

and the result is then denoted as $H^1(\Delta,\Omega)$ and $H^1_0(\Delta,\Omega)$, respectively.

Definition 3.7 (Bilinear Operator [24])**.** *Let B be the bilinear operator of the form*

$$B_{\Omega}(u,\nu) = \int_{\Omega} \langle \boldsymbol{\nabla} u, \boldsymbol{\nabla} \nu \rangle \, \mathrm{d}\vec{\mathbf{x}}\,. \tag{3.18}$$

Definition 3.8 (Trace Operator [24])**.** *There exist a continuous, linear trace operator $\gamma_0 \colon H^{\ell}_{loc}(\mathbb{R}^3) \to H^{\ell-1/2}(\Gamma)$ for $1/2 < \ell < 3/2$, such that*

$$\gamma_0 \nu = \nu\Big|_{\Gamma}, \quad \forall \nu \in C^0\Big(\mathbb{R}^3\Big). \tag{3.19}$$

Definition 3.9 (Conormal Derivative [24])**.** *Let Ω be a domain and $u \in H^2(\Omega)$. Then,*

$$\gamma_1 u \coloneqq \langle \vec{\mathbf{n}}, \gamma_0 \boldsymbol{\nabla} u \rangle \tag{3.20}$$

is the conormal derivative.

Definition 3.10 (Green's Formula [24])**.** *Let σ_{Ω} be defined as*

$$\sigma_{\Omega} = \begin{cases} 1, & \Omega = \Omega_{mag}, \\ -1, & \Omega = \Omega_0, \end{cases} \tag{3.21}$$

such that $\sigma_{\Omega}\vec{\mathbf{n}}$ denotes the outer normal relative to Ω. Green's first formula is defined as

$$\int_{\Omega} \Delta u \nu \, \mathrm{d}\vec{\mathbf{x}} = -\int_{\Omega} \langle \boldsymbol{\nabla} u, \boldsymbol{\nabla} \nu \rangle \, \mathrm{d}\vec{\mathbf{x}} + \sigma_{\Omega} \int_{\Gamma} \langle \vec{\mathbf{n}}, \boldsymbol{\nabla} u \rangle \, \nu \, \mathrm{d}S_{\vec{\mathbf{x}}}\,, \quad \forall u \in H^2(\Omega), \nu \in H^1(\Omega). \tag{3.22}$$

Green's second formula is defined as

$$\int_\Omega \Delta u\nu \,\mathrm{d}\vec{\mathbf{x}} - \int_\Omega u\Delta\nu \,\mathrm{d}\vec{\mathbf{x}} = \sigma_\Omega \left(\int_\Gamma \langle \vec{\mathbf{n}}, \boldsymbol{\nabla} u \rangle \, \nu \,\mathrm{d}S_{\vec{\mathbf{x}}} - \int_\Gamma u \, \langle \vec{\mathbf{n}}, \boldsymbol{\nabla}\nu \rangle \,\mathrm{d}S_{\vec{\mathbf{x}}} \right), \quad \forall u \in H^2(\Omega), \nu \in H^2(\Omega), \tag{3.23}$$

The following variational formulations are based on Sauter and Schwab [24].

3.2.2. *Abstract Problem 1.* Let $w_{\text{int}} \in H^1(\Delta, \Omega_{\text{mag}})$ and $f\colon \mathbb{R}^3 \to \mathbb{R}$, with $f \in L^2(\Omega_{\text{mag}})$. In order to state the variational formulation for Eq. (3.4), the equation is multiplied by a test function $\nu \in C_0^\infty(\Omega_{\text{mag}})$ and Green's formula is applied. This yields

$$B_{\Omega_{\text{mag}}}(w_{\text{int}}, \nu) - (\gamma_1 w_{\text{int}}, \gamma_0 \nu)_{L^2(\Gamma_{\text{mag}})} = (f, \nu)_{L^2(\Omega_{\text{mag}})}. \tag{3.24}$$

With $\gamma_0 \nu = 0$ we obtain

$$B_{\Omega_{\text{mag}}}(w_{\text{int}}, \nu) = (f, \nu)_{L^2(\Omega_{\text{mag}})}, \quad \forall \nu \in H_0^1(\Omega_{\text{mag}}). \tag{3.25}$$

Now, let $F(\cdot) = (f, \cdot)_{L^2(\Omega_{\text{mag}})} \in H^{-1}(\Omega_{\text{mag}})$ and $g_D = 0 \in H^{\frac{1}{2}}(\Gamma_{\text{mag}})$. The variational formulation then reads:
Find $w_{int} \in H_0^1(\Omega_{mag})$, such that

$$B_{\Omega_{mag}}(w_{int}, \nu) = F(\nu), \quad \forall \nu \in H_0^1(\Omega_{mag}). \tag{3.26}$$

Remark. *For $f = \boldsymbol{\nabla} \cdot \vec{\mathbf{M}}_2$ we get the variational formulation of Eq.* (3.6)*. Equivalently, the variational formulation of Eq.* (3.8) *is obtained for $f = \boldsymbol{\nabla} \cdot \left(\vec{\mathbf{M}}_1 - \vec{\mathbf{M}}_2 \right)$.*

3.2.3. *Abstract Problem 2.* We now derive the variational formulation for Eq. (3.5). Let $\hat{g} \in L^2(\Gamma_{\text{mag}})$ with $\hat{g} = g - \partial_{\vec{\mathbf{n}}} w_{\text{int}}$. The equation is multiplied by a test function $\nu \in C_0^\infty(\mathbb{R}^3)$. Integrating over Ω_{mag} and Ω_0 and applying Green's formula yields

$$B_{\Omega_{\text{mag}}}(w_{\text{ext}}, \nu) + B_{\Omega_0}(w_{\text{ext}}, \nu) = -(\hat{g}, \gamma_0 \nu)_{L^2(\Gamma_{\text{mag}})}. \tag{3.27}$$

Let $w_{\text{ext}} = \left(w_{\text{ext}}^{\Omega_{\text{mag}}}, w_{\text{ext}}^{\Omega_0} \right)$ be separated into a function defined in Ω_{mag} and one defined in Ω_0. Denote the same separation for ν. For

$$w_{\text{ext}}^{\Omega_{\text{mag}}}, \nu^{\Omega_{\text{mag}}} \in H^1(\Omega_{\text{mag}}),$$

and

$$w_{\text{ext}}^{\Omega_0}, \nu^{\Omega_0} \in H^1(\Delta, \Omega_0),$$

that satisfy $[w_{\text{ext}}] = 0, [\nu] = 0$, the sesquilinear Eq. (3.27) is well-defined. Therefore, the solution space, as well as the test function space, is defined as

$$W \coloneqq \left\{ w = \left(w^{\Omega_{\text{mag}}}, w^{\Omega_0} \right) \in \left(H^1(\Omega_{\text{mag}}), H^1(\Delta, \Omega_0) \right) \,\middle|\, [w] = 0 \right\}. \tag{3.28}$$

with the corresponding norm

$$\|w\|_W \coloneqq \sqrt{\|w\|^2_{H^1(\Omega_{\mathrm{mag}})} + \|w\|^2_{H^1(\Delta,\Omega_0)}}. \tag{3.29}$$

Additionally, let $F(\cdot) = -(g, \gamma_0 \cdot)_{L^2(\Gamma_{\mathrm{mag}})} \in W'$, with W' being the dual to W, be given. Then the variational formulation reads:
Find $w_{ext} \in W$, such that

$$B_{\Omega_{mag}}(w_{ext}, \nu) + B_{\Omega_0}(w_{ext}, \nu) = F(\nu), \quad \forall \nu \in W. \tag{3.30}$$

Remark. *For $\hat{g} = -\left(\vec{\mathbf{M}}_2 \cdot \vec{\mathbf{n}}\right) - \partial_{\vec{\mathbf{n}}} v_{int}|_{\Omega_2}$ we get the variational formulation of Eq.* (3.7)*. Equivalently, we get the variational formulation of Eq.* (3.9) *for $\hat{g} = -\left(\vec{\mathbf{M}}_1 - \vec{\mathbf{M}}_2\right) \cdot \vec{\mathbf{n}} - \partial_{\vec{\mathbf{n}}} u_{int}|_{\Omega_1}$.*

3.3. **Well-Posedness.** Now, the existence and uniqueness of the two abstract problems that we have derived will be stated. The weak formulations have already been derived in Section 3.2.

For the variational formulation in Abstract Problem 1, the Fredholm alternative is used, i.e. either the problem has a unique solution that depends continuously on the data, or zero is an eigenvalue of the operator associated with the bilinear form. In the case of a Poisson problem with zero Dirichlet boundary, the first case of the Fredholm alternative is always true [see, e.g., 24, Theorem (2.10.4.)] and therefore, together with the Lax-Milgram theorem a unique solution exists.

For the variational formulation in Abstract Problem 2 there exists a unique solution that depends continuously on the right-hand side [see, e.g., 24, Theorem (2.10.14.)].

We have shown, that the two abstract problems, and therefore the four subproblems Eqs. (3.6)–(3.9) are well-posed. Since we have also shown the equivalence of the subproblems and the coupled transmission problem Eq. (2.24), the computation of the scalar magnetic potential of a magnonic crystal is well-posed.

4. Numerical Method

Let us now derive the discretizations necessary to implement a scalar magnetic potential (SMP) solver for a magnonic crystal as described in Section 2.7. In this regard, we first define the mathematical tools needed for the discretization of the four subproblems Eqs. (3.6)–(3.9). Afterwards, the actual discretizations are explained.

4.1. Mathematical Preliminaries.

In order to efficiently solve the potential for spherical domains, the spherical harmonics are often used. These harmonic functions[3] are defined in terms of the associated Legendre polynomials.

Definition 4.1 (Associated Legendre Polynomials)**.** *Let $P_\ell^m\colon [-1,1] \to [-1,1]$, with $0 \leq m \leq \ell$. The associated Legendre polynomials are then defined by the recurrence scheme*

$$\begin{aligned} P_0^0(x) &= 1 \\ P_1^0(x) &= x \\ P_1^1(x) &= -\sqrt{1-x^2} \\ (\ell - m)P_\ell^m(x) &= x(2\ell-1)P_{\ell-1}^m(x) - (\ell+m-1)P_{\ell-2}^m(x). \end{aligned} \tag{4.1}$$

Remark. *For $m = 0$ the associated Legendre polynomials reduce to the ordinary Legendre polynomials. The superscript is then omitted, i.e. $P_i = P_\ell^0$.*

Theorem 4.1 (Identity Relation for the Legendre Polynomials [21])**.** *Let $x \in [-1,1]$. The ordinary Legendre polynomials $P_i, \quad i \geq 1$ have the identity relation*

$$\frac{d}{dx}\left((1-x^2)P_i'(x)\right) = -i(i+1)P_i(x). \tag{4.2}$$

Theorem 4.2 (Orthogonaliyt Property of the Legendre Polynomials [21])**.** *Let $x \in [-1,1]$. The ordinary Legendre polynomials $P_i, \quad i \geq 1$ and $P_j, \quad j \geq 1$ have the orthogonality property*

$$\int_{-1}^{1} P_i(x)P_j(x)dx = \frac{2\delta_{ij}}{2j+1}. \tag{4.3}$$

Definition 4.2 (Laplace's Real Spherical Harmonics)**.** *With the associated Legendre Polynomials the Laplace's real spherical harmonics $\mathcal{Y}_\ell^m\colon [0,\pi] \times [0,2\pi] \to \mathbb{R}$ are defined as*

$$\mathcal{Y}_\ell^m(\theta,\varphi) = \begin{cases} c(\ell,m)\cos(m\varphi)P_\ell^m(\cos\theta), & \text{if} \quad m > 0 \\ c(\ell,m)P_\ell^0(\cos\theta), & \text{if} \quad m = 0 \\ c(\ell,m)\sin(|m|\varphi)P_\ell^{|m|}(\cos\theta), & \text{if} \quad m < 0, \end{cases} \tag{4.4}$$

[3] A function that solves the Laplace equation is said to be harmonic.

with

$$c(\ell,m)=\begin{cases}\sqrt{2}\sqrt{\dfrac{2\ell+1}{4\pi}\dfrac{(\ell-m)!}{(\ell+m)!}}, & \text{if} \quad m>0\\ \sqrt{\dfrac{2\ell+1}{4\pi}}, & \text{if} \quad m=0\\ \sqrt{2}\sqrt{\dfrac{2\ell+1}{4\pi}\dfrac{(\ell-|m|)!}{(\ell+|m|)!}}, & \text{if} \quad m<0.\end{cases}$$

The following properties are the main reasons why the spherical harmonics are so important when developing Poisson solvers in spherical domains.

Remark. *The spherical harmonics fulfill*

$$r^2\Delta\mathcal{Y}_\ell^m(\theta,\varphi)=-\ell(\ell+1)\mathcal{Y}_\ell^m(\theta,\varphi). \tag{4.5}$$

and are a complete set of orthogonal functions, defined on a sphere's surface, and are therefore suited for an expansion of the solution to a Laplace or Poisson equation written in spherical coordinates. [21]

Remark. *The spherical harmonics are orthogonal w.r.t. the L^2 inner product [21]. It is*

$$\int_{\theta=0}^{\pi}\int_{\varphi=0}^{2\pi}\mathcal{Y}_\ell^m\mathcal{Y}_{\ell'}^{m'}\,d\varphi\,d\theta=\delta_{\ell\ell'}\delta_{mm'}, \tag{4.6}$$

with the usual Kronecker delta

$$\delta_{xy}=\begin{cases}1, & \text{if} \quad x=y\\ 0, & \text{otherwise.}\end{cases} \tag{4.7}$$

Remark. *The spherical harmonics are a complete set on $L^2(\mathbb{S}^2)$ with $\mathbb{S}^2$ being the surface of a unit ball. Hence, every $f\in L^2(\mathbb{S}^2)$ can be expressed in terms of spherical harmonics, i.e.*

$$f=\sum_{\ell=0}^{\infty}\sum_{m=-\ell}^{\ell}[f]_\ell^m\mathcal{Y}_\ell^m.$$

Since the spherical harmonics are orthonormal on the unit sphere, too, the coefficients can be obtained by

$$[f]_\ell^m=\int_{\mathbb{S}^2}f(\vec{\mathbf{s}})\mathcal{Y}_\ell^m(\vec{\mathbf{s}})\,\mathrm{d}\vec{\mathbf{s}}\,.$$

Since the functions are defined in spherical coordinates, the operators need to be given in spherical coordinates as well. Therefore, the following definitions are necessary.

Definition 4.3 (Divergence Operator in Spherical Coordinates)**.** *The divergence in spherical coordinates reads*

$$\boldsymbol{\nabla}\cdot\left(\vec{\mathbf{A}}\right)=\frac{1}{r^2}\partial_r\left(r^2A_r\right)+\frac{1}{r\sin\theta}\partial_\theta(A_\theta\sin\theta)+\frac{1}{r\sin\theta}\partial_\varphi A_\varphi \tag{4.8}$$

with A_r denoting the radial component of the vector A (the angular components are denoted accordingly). Here, the notation $\partial_x = \frac{\partial}{\partial x}$ is introduced.

Definition 4.4 (Laplace Operator in Spherical Coordinates)**.** *The Laplace operator in spherical coordinates reads*

$$\Delta f(\theta,\varphi,r) = \frac{1}{r^2}\partial_r\left(r^2\partial_r f\right) + \frac{1}{r^2\sin\theta}\partial_\theta\left(\sin\theta\ \partial_\theta f\right) + \frac{1}{r^2\sin^2\theta}\partial_{\varphi\varphi} f. \tag{4.9}$$

In this equation, the notation ∂_{xy} was introduced to mean $\frac{\partial^2}{\partial x\partial y}$.

For the efficient computation of the potential generated by many spheres, we utilize the following theorems.

Theorem 4.3 (Expansion)**.** *Let $\vec{\mathbf{x}}$ and $\vec{\mathbf{y}}$ be two points in $\mathbb{R}^3$ with spherical coordinates (r,θ,φ) and (ρ,α,β), respectively. Additionally, let γ denote the angle between the vectors that connect the origin with both points. Then, we have the identity*

$$\frac{1}{\|\vec{\mathbf{y}}-\vec{\mathbf{x}}\|} = \sum_{\ell=0}^{\infty} P_\ell(\cos\gamma)\begin{cases}\frac{\rho^\ell}{r^{\ell+1}}, & \text{if} \quad \rho < r\\ \frac{r^\ell}{\rho^{\ell+1}}, & \text{if} \quad \rho > r.\end{cases} \tag{4.10}$$

Theorem 4.4 (Addition theorem for Legendre polynomials [5])**.** *Let P and Q be points with spherical coordinates (r,θ,φ) and (ρ,α,β), respectively, and let γ be the angle between them. Then*

$$P_\ell(\cos\gamma) = \frac{4\pi}{2\ell+1}\sum_{m=-\ell}^{\ell}\mathcal{Y}_\ell^m(\alpha,\beta)\mathcal{Y}_\ell^m(\theta,\varphi) \tag{4.11}$$

The Eq. (3.6) is solved by a *spectral collocation method* using Chebyshev polynomials. The polynomials' extrema are the so called collocation points, i.e. the points at which the approximate solution determined. These polynomials and their extrema are now defined. Since we also need to interpolate between the collocation points, we define the Chebyshev polynomials of second kind, too.

Definition 4.5 (Chebyshev Polynomials of First Kind [20])**.** *The recursion scheme for evaluating Chebyshev polynomials of first kind reads*

$$\begin{aligned} T_0(x) &= 1\\ T_1(x) &= x\\ T_{n+1}(x) &= 2xT_n(x) - T_{n-1}(x), \quad n = 1,2,\ldots \end{aligned} \tag{4.12}$$

Definition 4.6 (Chebyshev Polynomials of Second Kind [20])**.** *The recursion scheme for evaluating Chebyshev polynomials of second kind*

reads

$$\begin{aligned} U_0(x) &= 1 \\ U_1(x) &= 2x \\ U_{n+1}(x) &= 2xU_n(x) - U_{n-1}(x), \quad n = 1, 2, \dots \end{aligned} \tag{4.13}$$

Definition 4.7 (Extrema of Chebyshev Polynomials [20])**.** *The extrema of $T_n(x)$ for $x \in [-1, 1]$ are*

$$x_k = \cos\left(\frac{k\pi}{n}\right), \quad k = 0, 1, \dots, n. \tag{4.14}$$

Remark. *The extrema of Chebyshev polynomials of first kind are also the zeros of the weighted Chebyshev polynomials of second kind [20], i.e.*

$$\left(1 - x^2\right) U_{n-1}(x). \tag{4.15}$$

Definition 4.8 (Interpolation at Extrema of Chebyshev Polynomials of First Kind [20])**.** *Let y_k denote the extrema of Chebyshev polynomials of first kind. Additionally, let $\sum''$ denote a sum in which the first and the last term is halved. The interpolation of a continuous function f on $[-1, 1]$ which values are known at the extrema y_k can be computed through*

$$p_n(x) = \sum_{i=0}^{n}{}'' \, c_i T_i(x). \tag{4.16}$$

Here, the coefficients are defined by

$$c_i = \frac{2}{n} \sum_{k=0}^{n}{}'' \, f(y_k) T_i(y_k). \tag{4.17}$$

In order to solve Eq. (3.7) we have to evaluate a derivative. Hence, we need the following definition.

Definition 4.9 (1^{st} Derivative of Chebyshev Polynomials [20])**.** *The derivative can be easily expressed in terms of Chebyshev polynomials of second kind, i.e.*

$$\begin{aligned} \frac{\mathrm{d}}{\mathrm{d}x} T_0(x) &= 0, \\ \frac{\mathrm{d}}{\mathrm{d}x} T_n(x) &= n U_{n-1}(x). \end{aligned} \tag{4.18}$$

Transmission problems like Eq. (3.7) are well studied and exact solutions exist. These solutions are built out of *single layer* and *double layer potentials*. In order to use these results we need the following definitions and relations.

Definition 4.10 (Single Layer Potential [24]). *Let $G\colon \mathbb{R}^3 \to \mathbb{R}$ be the Green's function of the Laplace operator in three dimensions, which reads*

$$G(\vec{\mathbf{x}}) = \frac{1}{4\pi\|\vec{\mathbf{x}}\|}. \tag{4.19}$$

Let Γ denote the boundary of a Lipshitz domain. A single layer potential is a functional of the form

$$\mathcal{S}[\sigma](\vec{\mathbf{x}}) = \int_\Gamma G(\vec{\mathbf{x}} - \vec{\mathbf{y}})\sigma(\vec{\mathbf{y}})\,\mathrm{d}\Gamma_{\vec{\mathbf{y}}}\,, \quad \vec{\mathbf{x}} \in \mathbb{R}^3 \setminus \Gamma, \tag{4.20}$$

with a density function $\sigma\colon \Gamma \to \mathbb{R}^3$.

Remark. *The single layer potential can be continuously extended across the boundary Γ [24] by*

$$\mathcal{V}[\sigma](\vec{\mathbf{x}}) = \int_\Gamma G(\vec{\mathbf{x}} - \vec{\mathbf{y}})\sigma(\vec{\mathbf{y}})\,\mathrm{d}\Gamma_{\vec{\mathbf{y}}}\,, \quad \vec{\mathbf{x}} \in \Gamma, \tag{4.21}$$

Definition 4.11 (Double Layer Potential [24]). *Set*

$$k(\vec{\mathbf{x}}, \vec{\mathbf{y}}) \coloneqq \langle \vec{\mathbf{n}}(\vec{\mathbf{y}}), \boldsymbol{\nabla}_{\vec{\mathbf{y}}} G(\vec{\mathbf{x}} - \vec{\mathbf{y}})\rangle = -\frac{\langle \vec{\mathbf{n}}(\vec{\mathbf{y}}), \vec{\mathbf{y}} - \vec{\mathbf{x}}\rangle}{4\pi\|\vec{\mathbf{y}} - \vec{\mathbf{x}}\|}. \tag{4.22}$$

The double layer potential is then defined as

$$\mathcal{D}[\theta](\vec{\mathbf{x}}) = \int_\Gamma k(\vec{\mathbf{x}}, \vec{\mathbf{y}})\theta(\vec{\mathbf{y}})\,\mathrm{d}\Gamma_{\vec{\mathbf{y}}}\,, \quad \forall \vec{\mathbf{x}} \in \mathbb{R}^3 \setminus \Gamma. \tag{4.23}$$

Theorem 4.5 (Jump Relations [24]). *For a bounded Lipshitz domain Ω with boundary Γ the following jump relations hold. Let $\mathcal{S}$ and $\mathcal{D}$ denote a single and double layer potential, respectively. For all $\phi \in H^{-\frac{1}{2}}(\Gamma)$ and $\Psi \in H^{\frac{1}{2}}(\Gamma)$, the relations*

$$\begin{aligned} [\mathcal{S}\phi] &= 0 \qquad [\mathcal{D}\Psi] = \Psi \quad \textit{in} \quad H^{\frac{1}{2}}(\Gamma) \\ [\gamma_1\mathcal{S}\phi] &= -\phi \quad [\gamma_1\mathcal{D}\Psi] = 0 \quad \textit{in} \quad H^{-\frac{1}{2}}(\Gamma) \end{aligned} \tag{4.24}$$

hold.

4.2. **Problem 1.** Let N be the number of non-overlapping spheres $B_{R_i}(\vec{\mathbf{c}}_i)$ centered at $\vec{\mathbf{c}}_i$ with radius R_i, $i = 1, \ldots, N$. We observe that the domains in Eq. (3.8) are strictly decoupled and therefore, the problem can be solved for each sphere separately. The solution to each sphere can then be combined into

$$u_{\mathrm{int}}(\vec{\mathbf{x}}) = \begin{cases} u_{\mathrm{int},i}(\vec{\mathbf{x}}), & \vec{\mathbf{x}} \in B_{R_i}(\vec{\mathbf{c}}_i), \quad i = 1, \ldots, N \\ 0, & \text{otherwise.} \end{cases} \tag{4.25}$$

In the following sequel we therefore describe the solution technique for one sphere.

Without loss of generality, we assume that the geometry is a unit ball centered at the origin $\Omega_1 = B_1(0)$. Whenever this is not the case we can define a linear mapping $\Psi\colon \mathbb{R}^3 \to \mathbb{R}^3$, s.t. $\vec{\mathbf{x}} \mapsto \frac{\vec{\mathbf{x}} - \vec{\mathbf{c}}_i}{R_i}$, that maps

the ball with center $\vec{\mathbf{c}}$ and radius R_i onto $B_1(0)$. Since the domain is a ball, it is natural to use spherical coordinates which we define as $(r, \theta, \phi) \in [0, \infty) \times [0, \pi] \times [0, 2\pi]$. Following the authors of Quan, Stamm, and Maday [21] we take as the solution ansatz a spherical harmonics expansion and define the subspace

$$\mathcal{V}_{N,\ell_{\max}} = \operatorname{span}\Big\{ r(1-r)P_i'(2r-1)\mathcal{Y}_\ell^m(\theta,\varphi) \Big| \; i = 1,\dots,N, \quad \ell = 0,\dots,\ell_{\max}, \quad |m| \le \ell \Big\} \subset H_0^1. \tag{4.26}$$

Here, N denotes the highest order of the first derivative of Legendre polynomials P_i' that discretize the radial part and $\ell_{\max}$ denote the highest degree of the real spherical harmonics $\mathcal{Y}_\ell^m$ that discretize the spherical part.

Let $[u_{\text{int}}]_{i,\ell,m} \in \mathbb{R}, \quad i = 1,\dots,N, \quad \ell = 0,\dots,\ell_{\max}, \quad |m| \le \ell$ be a coefficient and $z_i \colon [0,1] \to \mathbb{R}$ with $z_i(r) = r(1-r)P_i'(2r-1)$ the radial part of the functions in $\mathcal{V}$. The solution ansatz then reads

$$u_{\text{int}}(r,\theta,\varphi) \approx \sum_{i=1}^{N} \sum_{\ell=0}^{\ell_{\max}} \sum_{m=-\ell}^{\ell} [u_{\text{int}}]_{i,\ell,m} z_i(r) \mathcal{Y}_\ell^m(\theta,\varphi). \tag{4.27}$$

Inserting this ansatz together with the test functions $z_{i'}(r)\mathcal{Y}_{\ell'}^{m'}(\theta,\varphi) \in \mathcal{V}_{N,\ell_{\max}}$ into the weak formulation Eq. (3.26) yields

$$\begin{aligned} &\sum_{i=1}^{N} \sum_{\ell=0}^{\ell_{\max}} \sum_{m=-\ell}^{\ell} [u_{\text{int}}]_{i,\ell,m} \int_{B_1(0)} z_i(r)\mathcal{Y}_\ell^m(\theta,\varphi) z_{i'}(r)\mathcal{Y}_{\ell'}^{m'}(\theta,\varphi)\,\mathrm{d}V \\ &\quad = \int_{B_1(0)} \Big(\boldsymbol{\nabla}\cdot\vec{\mathbf{M}}_1(r,\theta,\varphi)\Big) z_{i'}(r)\mathcal{Y}_{\ell'}^{m'}(\theta,\varphi)\,\mathrm{d}V\,, \quad \forall i',\ell',m'. \end{aligned} \tag{4.28}$$

Henceforth, we drop the function's arguments to shorten the notation.

With the introduction of an index

$$k = N\Big(\ell^2 + \ell + m\Big) + i, \quad k \in \Big\{1, 2, \dots, N(\ell_{\max}+1)^2\Big\}, \tag{4.29}$$

Eq. (4.28) can be recast into matrix form, i.e.

$$Ax = b, \tag{4.30}$$

with $A \in \mathbb{R}^{N(\ell_{\max}+1)^2 \times N(\ell_{\max}+1)^2}$, $x \in \mathbb{R}^{N(\ell_{\max}+1)^2}$, and $b \in \mathbb{R}^{N(\ell_{\max}+1)^2}$. Note that A is a matrix with entries

$$A_{k,k'} = \int_{B_1(0)} \Big\langle \boldsymbol{\nabla} z_i \mathcal{Y}_\ell^m, \boldsymbol{\nabla} z_{i'} \mathcal{Y}_{\ell'}^{m'} \Big\rangle \,\mathrm{d}V\,. \tag{4.31}$$

The entries of b are computed through

$$b_{k'} = \int_{B_1(0)} \Big(\boldsymbol{\nabla}\cdot\vec{\mathbf{M}}_1\Big) z_{i'}\mathcal{Y}_{\ell'}^{m'}\,\mathrm{d}V\,, \tag{4.32}$$

and after solving the linear system of equation we obtain the coefficients

$$x_k = [u_{\text{int}}]_{i,\ell,m}. \tag{4.33}$$

It remains to compute the integrals in Eqs. (4.31) and (4.32). For the latter integral we construct a tensorized quadrature rule by combining the Gauß-Lebedev quadrature for the spherical part with the Gauß-Legendre quadrature for the radial part of the functions. Therefore, we evaluate for each i', ℓ', m'

$$\begin{aligned}(4.34)\quad &\int_{B_1(0)} \left(\boldsymbol{\nabla} \cdot \vec{\mathbf{M}}_1\right) z_{i'} \mathcal{Y}_{\ell'}^{m'} \,\mathrm{d}V \\ &\qquad \approx \sum_{i=1}^{M_{\mathrm{leg}}} \sum_{j=1}^{M_{\mathrm{leb}}} w_i^{\mathrm{leg}} w_j^{\mathrm{leb}} \left(\boldsymbol{\nabla} \cdot \vec{\mathbf{M}}_1(r_i, \theta_j, \varphi_j)\right) z_{i'}(r_i) \mathcal{Y}_{\ell'}^{m'}(\theta_j, \varphi_j).\end{aligned}$$

In order to compute the integral in Eq. (4.31) we first utilize some orthogonality properties of the spherical harmonics and the Legendre polynomials. Therefore, we multiply out the integrand and separate the radial from the spherical functions, i.e.

$$\begin{aligned}(4.35)\quad &\int_{B_1(0)} \left\langle \boldsymbol{\nabla} z_i \mathcal{Y}_\ell^m, \boldsymbol{\nabla} z_{i'} \mathcal{Y}_{\ell'}^{m'} \right\rangle \mathrm{d}V = \int_0^1 \langle \boldsymbol{\nabla} z_i, \boldsymbol{\nabla} z_{i'} \rangle \int_{\mathbb{S}^2} \mathcal{Y}_\ell^m \mathcal{Y}_{\ell'}^{m'} \,\mathrm{d}S \,\mathrm{d}r \\ &\qquad + \int_0^1 z_i z_{i'} \int_{\mathbb{S}^2} \left\langle \boldsymbol{\nabla} \mathcal{Y}_\ell^m, \boldsymbol{\nabla} \mathcal{Y}_{\ell'}^{m'} \right\rangle \mathrm{d}S \,\mathrm{d}r \,.\end{aligned}$$

Together with the orthonormality condition Eq. (4.6) and the identity Eq. (4.5) we get

$$\begin{aligned}(4.36)\quad &\int_{B_1(0)} \left\langle \boldsymbol{\nabla} z_i \mathcal{Y}_\ell^m, \boldsymbol{\nabla} z_{i'} \mathcal{Y}_{\ell'}^{m'} \right\rangle \mathrm{d}V = \int_0^1 \langle \boldsymbol{\nabla} z_i, \boldsymbol{\nabla} z_{i'} \rangle \,\delta_{\ell\ell'} \delta_{mm'} \,\mathrm{d}r \\ &\qquad + \frac{\ell(\ell+1)}{r^2} \int_0^1 z_i z_{i'} \,\mathrm{d}r \,\delta_{\ell\ell'} \delta_{mm'}.\end{aligned}$$

With the substitution $\zeta = 2r - 1$ we finally use the identity Eq. (4.2) and apply the orthogonality property of the Legendre polynomials in Eq. (4.3) to get

$$\begin{aligned}(4.37)\quad &\int_{B_1(0)} \left\langle \boldsymbol{\nabla} z_i \mathcal{Y}_\ell^m, \boldsymbol{\nabla} z_{i'} \mathcal{Y}_{\ell'}^{m'} \right\rangle \mathrm{d}V = \frac{i^2(i+1)^2}{4(2i+1)} \delta_{ii'} \delta_{\ell\ell'} \delta_{mm'} \\ &\qquad + \frac{\ell(\ell+1)}{r^2} \int_0^1 z_i z_{i'} \,\mathrm{d}r \,\delta_{\ell\ell'} \delta_{mm'}.\end{aligned}$$

Therefore, the computation of the matrix A reduces to

$$(4.38)\qquad A_{kk'} = \frac{i^2(i+1)^2}{4(2i+1)} \delta_{ii'} \delta_{\ell\ell'} \delta_{mm'} + \frac{\ell(\ell+1)}{r^2} \int_0^1 z_i z_{i'} \,\mathrm{d}r \,\delta_{\ell\ell'} \delta_{mm'},$$

and therefore, we get a block-diagonal matrix. Blocks w.r.t. radial index i and diagonal w.r.t. the angular indices ℓ, and m. The integral is again evaluated using the Gauß-Legendre quadrature, i.e.

$$(4.39)\qquad \int_0^1 z_i(r) z_{i'}(r) \,\mathrm{d}r \approx \sum_{j=1}^{M_{\mathrm{leg}}} w_j z_i(r_j) z_{i'}(r_j),$$

with the quadrature weights w_j and points r_j.

After solving the Eq. (4.30) for x, the solution to Eq. (3.8) is given by

$$u_{\text{int}}(r,\theta,\varphi) = \sum_{i=1}^{N} \sum_{\ell=0}^{\ell_{\max}} \sum_{m=-\ell}^{\ell} [u_{\text{int}}]_{i,\ell,m} z_i(r) \mathcal{Y}_\ell^m(\theta,\varphi). \tag{4.40}$$

We also need the derivative in direction of the outward pointing unit normal, which for the ball in spherical coordinates is just the derivative w.r.t. the radius, i.e. $\partial_{\vec{\mathbf{n}}} \cdot |_{\Omega_1} = \partial_r \cdot |_{\Omega_1} = \frac{\partial}{\partial r} \cdot |_{\Omega_1}$. Applied to Eq. (4.40) this results in

$$\partial_r u_{\text{int}}(r,\theta,\varphi) = \sum_{i=1}^{N} \sum_{\ell=0}^{\ell_{\max}} \sum_{m=-\ell}^{\ell}{}'' [u_{\text{int}}]_{i,\ell,m} \partial_r z_i(r) \mathcal{Y}_\ell^m(\theta,\varphi), \tag{4.41}$$

with

$$\partial_r z_i(r) = (-2r+1) P_i'(2r-1) + \left(r - r^2\right) P_i(2r-1) 2. \tag{4.42}$$

4.3. **Problem 2.** Following the monograph "Boundary Element Methods" of Sauter and Schwab [24, Section 3.4.1.3] the solution of a transmission problem of the form

$$\begin{aligned} \Delta u_{\text{ext}} &= 0, \quad \text{in} \quad \Omega_1 \\ \Delta u_{\text{ext}} &= 0, \quad \text{in} \quad \Omega_0 \cup \Omega_2 \\ [u_{\text{ext}}] &= g_D, \quad \text{on} \quad \Gamma_1 \\ [\gamma_1 u_{\text{ext}}] &= g_N, \quad \text{on} \quad \Gamma_1, \end{aligned} \tag{4.43}$$

is given by

$$u_{\text{ext}} = \mathcal{S} g_N + \mathcal{D} g_D. \tag{4.44}$$

In view of Eq. (3.9) we are dealing with a zero Dirichlet jump condition, i.e. $g_D = 0$, and the Neumann jump condition g_N is known. In our case, the boundary is actually composed of multiple spheres. Considering N spheres, we now denote by $\Gamma_{1,i}, i = 1,\dots,N$ and $\sigma_i, i = 1,\dots,N$ the boundary and the Neumann jump condition of the i-th ball. The solution therefore reads

$$u_{\text{ext}}(\vec{\mathbf{x}}) = \mathcal{S}(\vec{\mathbf{x}}) = \sum_{i=1}^{N} \int_{\Gamma_{1,i}} \frac{\sigma_i(\vec{\mathbf{y}})}{4\pi \|\vec{\mathbf{y}} - \vec{\mathbf{x}}\|} \, \mathrm{d}\vec{\mathbf{y}}\,, \quad \vec{\mathbf{x}} \in \mathbb{R}^3, \tag{4.45}$$

with

$$\sigma_i(\vec{\mathbf{y}}) = -\left(\vec{\mathbf{M}}_{1,i}(\vec{\mathbf{y}}) - \vec{\mathbf{M}}_2(\vec{\mathbf{y}})\right) \cdot \vec{\mathbf{n}}_i(\vec{\mathbf{y}}) - \partial_{\vec{\mathbf{n}}_i} u_{\text{int},i}(\vec{\mathbf{y}}) \Big|_{\Omega_{1,i}}. \tag{4.46}$$

For each sphere, an integral of the form

$$\int_{\Gamma_{1,i}} \frac{\sigma_i(\vec{\mathbf{y}})}{4\pi \|\vec{\mathbf{y}} - \vec{\mathbf{x}}\|} \, \mathrm{d}\vec{\mathbf{y}} \tag{4.47}$$

therefore has to be evaluated.

In the following paragraphs, we explain the evaluation for a unit sphere. Hence, the actual evaluation point $\vec{\mathbf{x}}$ needs to be scaled onto the unit sphere. Therefore, we define the mapping $\Psi_i \colon \mathbb{R}^3 \to \mathbb{R}^3, \quad \vec{\mathbf{x}} \mapsto \frac{(\vec{\mathbf{x}}-\vec{\mathbf{c}}_i)}{R_i}$, with $\vec{\mathbf{c}}_i$ denoting the i-th ball's center. Let us define

$$\vec{\hat{\mathbf{y}}} \coloneqq \Psi_i(\vec{\mathbf{y}}) = \frac{\vec{\mathbf{y}} - \vec{\mathbf{c}}_i}{R_i} \tag{4.48}$$

and

$$\vec{\hat{\mathbf{x}}} \coloneqq \Psi_i(\vec{\mathbf{x}}) = \frac{\vec{\mathbf{x}} - \vec{\mathbf{c}}_i}{R_i}, \tag{4.49}$$

such that

$$\hat{\sigma}_i\Big(\vec{\hat{\mathbf{y}}}\Big) \coloneqq \sigma_i\Big(R_i\vec{\hat{\mathbf{y}}} + \vec{\mathbf{c}}_i\Big) \tag{4.50}$$

Therefore, we get

$$\int_{\Gamma_{1,i}} \frac{\sigma_i(\vec{\mathbf{y}})}{4\pi\|\vec{\mathbf{y}} - \vec{\mathbf{x}}\|}\,\mathrm{d}\vec{\mathbf{y}} = \int_{\mathbb{S}^2} \frac{\hat{\sigma}_i\Big(\vec{\hat{\mathbf{y}}}\Big)}{4\pi\Big\|\vec{\hat{\mathbf{y}}} - \vec{\hat{\mathbf{x}}}\Big\|}\,\mathrm{d}\vec{\hat{\mathbf{y}}} \tag{4.51}$$

Let $\hat{\sigma}_i \in L^2(\mathbb{S}^2)$ and $(1, \theta, \phi)$ be the spherical coordinates of $\vec{\hat{\mathbf{y}}}$. Then, we expand the function in terms of spherical harmonics and truncate at $\ell_{\max}$, i.e.

$$\sigma_i\Big(R_i\vec{\hat{\mathbf{y}}} + \vec{\mathbf{c}}_i\Big) = \hat{\sigma}_i\Big(\vec{\hat{\mathbf{y}}}\Big) \approx \sum_{\ell=0}^{\ell_{\max}} \sum_{m=-\ell}^{\ell} [\sigma_i]_\ell^m \mathcal{Y}_\ell^m(\theta, \varphi), \quad \vec{\hat{\mathbf{y}}} \in \mathbb{S}^2. \tag{4.52}$$

The coefficients $[\sigma_i]_\ell^m$ are obtained through

$$[\sigma_i]_\ell^m = \int_{\mathbb{S}^2} \hat{\sigma}_i(\vec{\mathbf{s}})\mathcal{Y}_\ell^m(\vec{\mathbf{s}})\,\mathrm{d}\vec{\mathbf{s}} = \int_{\mathbb{S}^2} \sigma_i(R_i\vec{\mathbf{s}} + \vec{\mathbf{c}}_i)\mathcal{Y}_\ell^m(\vec{\mathbf{s}})\,\mathrm{d}\vec{\mathbf{s}}\,. \tag{4.53}$$

The efficient approximation of this integral is done using the Gauß-Lebedev quadrature scheme as initially introduced by Lebedev and Laikov [18].

Let now $\Big(r^i_{\vec{\hat{\mathbf{x}}}}, \theta^i_{\vec{\hat{\mathbf{x}}}}, \varphi^i_{\vec{\hat{\mathbf{x}}}}\Big)$ and $(r_{\vec{\mathbf{y}}}, \theta_{\vec{\mathbf{y}}}, \varphi_{\vec{\mathbf{y}}})$ denote the spherical coordinates of $\vec{\hat{\mathbf{x}}}$ and $\vec{\hat{\mathbf{y}}}$, respectively. Since we are dealing with an integral over the sphere's surface, we can expand $\frac{1}{\Big\|\vec{\mathbf{y}} - \vec{\hat{\mathbf{x}}}\Big\|}$ by means of a multipole expansion around the sphere's center using Theorems 4.3 and 4.4, and obtain after a truncation at $\ell_{\max}$

$$\frac{1}{\Big\|\vec{\mathbf{y}} - \vec{\hat{\mathbf{x}}}\Big\|} \approx \sum_{\ell=0}^{\ell_{\max}} \sum_{m=-\ell}^{\ell} \frac{4\pi}{2\ell+1} c\Big(r^i_{\vec{\hat{\mathbf{x}}}}\Big)\mathcal{Y}_\ell^m(\theta_{\vec{\mathbf{y}}}, \varphi_{\vec{\mathbf{y}}})\mathcal{Y}_\ell^m\Big(\theta^i_{\vec{\hat{\mathbf{x}}}}, \varphi^i_{\vec{\hat{\mathbf{x}}}}\Big), \tag{4.54}$$

with

$$c\Big(r^i_{\vec{\hat{\mathbf{x}}}}\Big) = \begin{cases} \frac{1}{{r^i_{\vec{\hat{\mathbf{x}}}}}^{\ell+1}}, & \text{if} \quad r^i_{\vec{\hat{\mathbf{x}}}} > 1 \\ 1, & \text{if} \quad r^i_{\vec{\hat{\mathbf{x}}}} = 1 \\ {r^i_{\vec{\hat{\mathbf{x}}}}}^{\ell}, & \text{if} \quad r^i_{\vec{\hat{\mathbf{x}}}} < 1. \end{cases} \tag{4.55}$$

Inserting Eqs. (4.52) and (4.54) into Eq. (4.51) yields

$$\begin{aligned}(4.56)\quad &\int_{\Gamma_{1,i}} \frac{\sigma_i(\vec{\mathbf{y}})}{4\pi\|\vec{\mathbf{y}}-\vec{\mathbf{x}}\|}\,\mathrm{d}\vec{\mathbf{y}} \\ &= \int_{\mathbb{S}^2} \frac{\hat{\sigma}_i(\vec{\mathbf{y}})}{4\pi\left\|\vec{\mathbf{y}}-\vec{\hat{\mathbf{x}}}\right\|}\,\mathrm{d}\vec{\mathbf{y}} \approx \int_{\mathbb{S}^2} \sum_{\ell=0}^{\ell_{\max}} \sum_{m=-\ell}^{\ell} [\sigma_i]_\ell^m \mathcal{Y}_\ell^m(\theta_{\vec{\mathbf{y}}},\varphi_{\vec{\mathbf{y}}}) \\ &\qquad \cdot \sum_{\ell'=0}^{\ell'_{\max}} \sum_{m'=-\ell'}^{\ell'} \frac{\mathcal{Y}_{\ell'}^{m'}(\theta_{\vec{\mathbf{y}}},\varphi_{\vec{\mathbf{y}}})}{2\ell'+1} c\Big(r^i_{\hat{\vec{\mathbf{x}}}}\Big) \mathcal{Y}_{\ell'}^{m'}\Big(\theta^i_{\hat{\vec{\mathbf{x}}}},\varphi^i_{\hat{\vec{\mathbf{x}}}}\Big)\,\mathrm{d}\theta_{\vec{\mathbf{y}}}\,\mathrm{d}\varphi_{\vec{\mathbf{y}}}\,.\end{aligned}$$

Rewriting the equation yields

$$\begin{aligned}(4.57)\quad \int_{\Gamma_{1,i}} \frac{\sigma_i(\vec{\mathbf{y}})}{4\pi\|\vec{\mathbf{y}}-\vec{\mathbf{x}}\|}\,\mathrm{d}\vec{\mathbf{y}} &\approx \sum_{\ell=0}^{\ell_{\max}} \sum_{m=-\ell}^{\ell} [\sigma_i]_\ell^m \sum_{\ell'=0}^{\ell'_{\max}} \sum_{m'=-\ell'}^{\ell'} \frac{\mathcal{Y}_{\ell'}^{m'}\Big(\theta^i_{\hat{\vec{\mathbf{x}}}},\varphi^i_{\hat{\vec{\mathbf{x}}}}\Big)}{2\ell'+1} \\ &\qquad \cdot c\Big(r^i_{\hat{\vec{\mathbf{x}}}}\Big) \int_{\mathbb{S}^2} \mathcal{Y}_\ell^m(\theta_{\vec{\mathbf{y}}},\varphi_{\vec{\mathbf{y}}}) \mathcal{Y}_{\ell'}^{m'}(\theta_{\vec{\mathbf{y}}},\varphi_{\vec{\mathbf{y}}})\,\mathrm{d}\theta_{\vec{\mathbf{y}}}\,\mathrm{d}\varphi_{\vec{\mathbf{y}}}\,,\end{aligned}$$

and we can again use the spherical harmonics orthogonality to get

$$(4.58)\qquad \int_{\Gamma_{1,i}} \frac{\sigma_i(\vec{\mathbf{y}})}{4\pi\|\vec{\mathbf{y}}-\vec{\mathbf{x}}\|}\,\mathrm{d}\vec{\mathbf{y}} \approx \sum_{\ell=0}^{\ell_{\max}} \sum_{m=-\ell}^{\ell} [\sigma_i]_\ell^m \frac{c\Big(r^i_{\hat{\vec{\mathbf{x}}}}\Big)}{2\ell+1} \mathcal{Y}_\ell^m\Big(\theta^i_{\hat{\vec{\mathbf{x}}}},\varphi^i_{\hat{\vec{\mathbf{x}}}}\Big)$$

We can now evaluate the potential for multiple spheres through

$$\begin{aligned}(4.59)\quad u_{\mathrm{ext}}(\vec{\mathbf{x}}) &\approx \sum_{\ell=0}^{\ell_{\max}} \sum_{m=-\ell}^{\ell} \sum_{i=1}^{N} [\sigma_i]_\ell^m \frac{c\Big(r^i_{\hat{\vec{\mathbf{x}}}}\Big)}{2\ell+1} \mathcal{Y}_\ell^m\Big(\theta^i_{\hat{\vec{\mathbf{x}}}},\varphi^i_{\hat{\vec{\mathbf{x}}}}\Big) \\ &= \sum_{\ell=0}^{\ell_{\max}} \sum_{m=-\ell}^{\ell} [\Phi_i]_\ell^m c\Big(r^i_{\hat{\vec{\mathbf{x}}}}\Big) \mathcal{Y}_\ell^m\Big(\theta^i_{\hat{\vec{\mathbf{x}}}},\varphi^i_{\hat{\vec{\mathbf{x}}}}\Big),\end{aligned}$$

with the so called multipole moment $[\Phi]_\ell^m \in \mathbb{R}$ defined as

$$(4.60)\qquad [\Phi_i]_\ell^m = \sum_{i=1}^{N} \frac{[\sigma_i]_\ell^m}{2\ell+1}.$$

However, we might want to evaluate the potential at multiple points $\vec{\mathbf{x}}_j, \quad j = 1,\ldots,M$, i.e.

$$(4.61)\quad u_{\mathrm{ext}}(\vec{\mathbf{x}}_j) = \mathcal{S}(\vec{\mathbf{x}}_j) = \sum_{i=1}^{N} \int_{\Gamma_{1,i}} \frac{\sigma_i(\vec{\mathbf{y}})}{4\pi\|\vec{\mathbf{y}}-\vec{\mathbf{x}}_j\|}\,\mathrm{d}\vec{\mathbf{y}}\,, \quad \forall j = 1,\ldots,M.$$

With the multipole moment from Eq. (4.60) we can approximate this

$$(4.62)\qquad u_{\mathrm{ext}}(\vec{\mathbf{x}}_j) \approx \sum_{\ell=0}^{\ell_{\max}} \sum_{m=-\ell}^{\ell} [\Phi]_\ell^m c\Big(r^i_{\hat{\vec{\mathbf{x}}}_j}\Big) \mathcal{Y}_\ell^m\Big(\theta^i_{\hat{\vec{\mathbf{x}}}_j},\varphi^i_{\hat{\vec{\mathbf{x}}}_j}\Big), \quad \forall j = 1,\ldots,M,$$

which expands to

(4.63)
$$u_{\text{ext}}(\vec{\mathbf{x}}_j) \approx \sum_{\ell=0}^{\ell_{\max}} \sum_{m=-\ell}^{\ell} [\Phi]_\ell^m \frac{1}{r^{i}_{\hat{\vec{\mathbf{x}}}_j \ \ell+1}} \mathcal{Y}_\ell^m\Big(\theta^i_{\hat{\vec{\mathbf{x}}}_j}, \varphi^i_{\hat{\vec{\mathbf{x}}}_j}\Big), \quad \forall j = 1, \dots, M,$$

if $\vec{\mathbf{x}}_j > \vec{\mathbf{y}}_i, \quad i = 1, \dots, N$.

Obviously, the computational cost would lie in $\mathcal{O}(NM)$. And exactly in this case, the fast multipole method (FMM) by Greengard and Rokhlin [10] excels. With this method it is possible to reduce the computational cost up to $\mathcal{O}(N)$ (see Appendix A for a sketch of the FMM). The *Matlab* code developed during this Thesis utilizes the *ScalFMM* library from Blanchard et al. [6].

4.4. **Problem 3.** In order to solve Eq. (3.6) a *spectral collocation method* is implemented. Therefore, we discretize the Laplacian using a differentiation matrix, valid for the Chebyshev polynomials, according to Mason and Handscomb [20]. Let N denote the total degree of Chebyshev polynomials and $y_k \in [-1, 1]$ the $N + 1$ extrema. The differentiation matrix $D \in \mathbb{R}^{(N+1)\times(N+1)}$ can then be computed by

(4.64)
$$\begin{aligned}
d_{j,k} &= \frac{(-1)^{k-j}}{y_j - y_k}, && 0 < j \neq k < N \\
d_{k,k} &= -\frac{1}{2}\frac{y_k}{1 - y_N^2}, && 0 < k < N \\
d_{0,k} &= 2\frac{(-1)^k}{1 - y_k}, && 0 < k < N \\
d_{k,0} &= \frac{1}{2}\frac{(-1)^k}{1 - y_k}, && 0 < k < N \\
d_{k,N} &= \frac{1}{2}\frac{(-1)^{N-k}}{1 + y_k}, && 0 < k < N \\
d_{N,k} &= -2\frac{(-1)^{N-k}}{1 + y_k}, && 0 < k < N \\
d_{0,0} &= \frac{1}{6}\Big(1 + 2N^2\Big) \\
d_{N,N} &= -\frac{1}{6}\Big(1 + 2N^2\Big) \\
d_{0,N} &= \frac{1}{2}(-1)^N \\
d_{N,0} &= -\frac{1}{2}(-1)^N,
\end{aligned}$$

where $d_{i,j}$ denote the entries of D.

In order to enforce the homogeneous Dirichlet boundary condition, the first and last row and column of D are removed and the nodal

values of the solution are imposed directly to be zero. Therefore, we obtain a new matrix $D' \in \mathbb{R}^{(N-1)\times(N-1)}$. With this representation we can formulate the discrete Laplacian $\tilde{L} \in \mathbb{R}^{(N-1)^3\times(N-1)^3}$ in three dimensions as

$$\tilde{L} = (I \otimes I) \otimes D'^2 + \left(I \otimes D'^2\right) \otimes I + \left(D'^2 \otimes I\right) \otimes I, \tag{4.65}$$

using the Kronecker tensor product $\otimes$ and the identity matrix I. Let $\tilde{f} \in \mathbb{R}^{(N-1)^3}$ with $\tilde{f} \coloneqq \boldsymbol{\nabla} \cdot \vec{\mathbf{M}}_2(\vec{\mathbf{y}}_{klm})$ be the right-hand side of Eq. (3.6) evaluated at the tensorized grid of extrema of the Chebyshev polynomials of first kind, i.e. $\vec{\mathbf{y}}_{klm} = (y_k, y_l, y_m)^T, \quad k,l,m = 1,\dots,N-1$. Notice, that these are only the inner extrema. Now, v_{int} can be approximated at these inner extrema by just solving the system of linear equations

$$\tilde{L}\tilde{v}'_{\text{int}} = \tilde{f}. \tag{4.66}$$

Here, $\tilde{v}'_{\text{int}}$ denotes the approximation of v_{int} at the grid of inner extrema.

Now, the boundary condition is enforced. Since in Eq. (3.6) the Dirichlet boundary is zero, we set

$$[\tilde{v}_{\text{int}}]_{k,l,m} = \begin{cases} 0, & \text{if} \quad k = 0 \vee l = 0 \vee m = 0 \\ 0, & \text{if} \quad k = N \vee l = N \vee m = N \\ [\tilde{v}'_{\text{int}}]_{k,l,m}, & \text{otherwise,} \end{cases} \tag{4.67}$$

with $\tilde{v}_{\text{int}} \in \mathbb{R}^{(N+1)^3}$. However, we are also interested in the solution at intermediate points. Therefore, we use the interpolation formula stated in Definition 4.8, which in three dimensions, i.e. $\vec{\mathbf{x}} = (x_1, x_2, x_3)^T$, extends to

$$p_N(\vec{\mathbf{x}}) = \sum_{i=0}^{N}{}'' \sum_{j=0}^{N}{}'' \sum_{k=0}^{N}{}'' c_{i,j,k} T_i(x_1) T_j(x_2) T_k(x_3), \tag{4.68}$$

with the coefficients

$$c_{i,j,k} = \frac{8}{N^3} \sum_{p=0}^{N}{}'' \sum_{q=0}^{N}{}'' \sum_{r=0}^{N}{}'' [\tilde{v}_{\text{int}}]_{p,q,r} T_i(y_p) T_j(y_q) T_k(y_r). \tag{4.69}$$

In order to solve Problem 4 we also need to be able to compute the derivative in direction of the outward pointing unit normal. With the coefficients from Eq. (4.69), the gradient $\boldsymbol{\nabla} = \left(\frac{\mathrm{d}}{\mathrm{d}x_1}, \frac{\mathrm{d}}{\mathrm{d}x_2}, \frac{\mathrm{d}}{\mathrm{d}x_3}\right)^T$ reads

$$\begin{aligned} \frac{\mathrm{d}}{\mathrm{d}x_1} p_N(\vec{\mathbf{x}}) &= \sum_{i=0}^{N}{}'' \sum_{j=0}^{N}{}'' \sum_{k=0}^{N}{}'' c_{i,j,k} \frac{\mathrm{d}}{\mathrm{d}x_1} T_i(x_1) T_j(x_2) T_k(x_3) \\ \frac{\mathrm{d}}{\mathrm{d}x_2} p_N(\vec{\mathbf{x}}) &= \sum_{i=0}^{N}{}'' \sum_{j=0}^{N}{}'' \sum_{k=0}^{N}{}'' c_{i,j,k} T_i(x_1) \frac{\mathrm{d}}{\mathrm{d}x_2} T_j(x_2) T_k(x_3) \\ \frac{\mathrm{d}}{\mathrm{d}x_3} p_N(\vec{\mathbf{x}}) &= \sum_{i=0}^{N}{}'' \sum_{j=0}^{N}{}'' \sum_{k=0}^{N}{}'' c_{i,j,k} T_i(x_1) T_j(x_2) \frac{\mathrm{d}}{\mathrm{d}x_3} T_k(x_3), \end{aligned} \tag{4.70}$$

with the derivative of the Chebyshev polynomials as given in Definition 4.9. So finally, we can solve Problem 3, i.e.

$$v_{\text{int}}(\vec{\mathbf{x}}) = p_n(\vec{\mathbf{x}}), \tag{4.71}$$

and compute its gradient $\boldsymbol{\nabla} v_{\text{int}}$ through Eq. (4.70).

4.5. **Problem 4.** We have already stated that Eq. (3.7) is a transmission problem and has an exact solution given by the single layer potential

$$v_{\text{ext}}(\vec{\mathbf{x}}) = \mathcal{S}[\sigma](\vec{\mathbf{x}}) = \int_{\Gamma_2} \frac{\sigma(\vec{\mathbf{y}})}{4\pi\|\vec{\mathbf{y}} - \vec{\mathbf{x}}\|} \,\mathrm{d}\vec{\mathbf{y}}\,, \tag{4.72}$$

with $\sigma(\vec{\mathbf{y}})$ being defined as

$$\sigma(\vec{\mathbf{y}}) = -\Big(\vec{\mathbf{M}}_2(\vec{\mathbf{y}}) \cdot \vec{\mathbf{n}}(\vec{\mathbf{y}})\Big) - \partial_{\vec{\mathbf{n}}} v_{\text{int}}(\vec{\mathbf{y}})\Big|_{\Omega_2}. \tag{4.73}$$

Here, $\partial_{\vec{\mathbf{n}}} v_{\text{int}}\,|_{\Omega_2}$ is the gradient from Section 4.4 multiplied by the outward pointing unit normal and evaluated from the inside of the domain Ω_2. If we separate the cuboid's six faces, the integral reads

$$\int_{\Gamma_2} \frac{\sigma(\vec{\mathbf{y}})}{4\pi\|\vec{\mathbf{y}} - \vec{\mathbf{x}}\|} \,\mathrm{d}\vec{\mathbf{y}} = \sum_{i=1}^{6} \int_{\Gamma_{2,i}} \frac{\sigma(\vec{\mathbf{y}})}{4\pi\|\vec{\mathbf{y}} - \vec{\mathbf{x}}\|} \,\mathrm{d}\vec{\mathbf{y}}\,, \tag{4.74}$$

with $\Gamma_{2,i}$ being the i-th face. This equation has a singular integrand at $\vec{\mathbf{x}} = \vec{\mathbf{y}}$, i.e. if we want to compute the potential on one of the cuboid's faces, the usual Gaussian quadrature scheme cannot be applied. In this case, we need to subtract the singularity.

Assume that the evaluation point $\vec{\mathbf{x}}$ does not lie on a face of the cuboid. Then for $i = 1, \ldots, 6$ the integral is computed using the usual Gauß-Legendre quadrature rule, i.e.

$$\int_{\Gamma_{2,i}} \frac{\sigma(\vec{\mathbf{y}})}{\|\vec{\mathbf{y}} - \vec{\mathbf{x}}\|} \,\mathrm{d}\vec{\mathbf{y}} \approx \sum_{i=1}^{N} \sum_{j=1}^{M} w_{ij} \frac{\sigma(\vec{\mathbf{y}}_{ij})}{\|\vec{\mathbf{y}}_{ij} - \vec{\mathbf{x}}\|}. \tag{4.75}$$

Here, w_{ij} and $\vec{\mathbf{y}}_{ij}$ are the tensorized Gauß-Legendre quadrature weights and points on the cuboid's face, respectively.

Now, assume an evaluation on one of the cuboid's faces. We are interested in solving an integral equation of the form

$$F(\vec{\mathbf{x}}) = \int_{\Gamma_{2,i}} \frac{f(\vec{\mathbf{y}})}{\|\vec{\mathbf{y}} - \vec{\mathbf{x}}\|} \,\mathrm{d}\vec{\mathbf{y}}\,. \tag{4.76}$$

Adding zero intelligently as in Acton [2] yields

$$\begin{aligned} F(\vec{\mathbf{x}}) &= \int_{\Gamma_{2,i}} \frac{f(\vec{\mathbf{y}}) - f(\vec{\mathbf{x}}) + f(\vec{\mathbf{x}})}{\|\vec{\mathbf{y}} - \vec{\mathbf{x}}\|} \,\mathrm{d}\vec{\mathbf{y}} \\ &= \int_{\Gamma_{2,i}} \frac{f(\vec{\mathbf{y}}) - f(\vec{\mathbf{x}})}{\|\vec{\mathbf{y}} - \vec{\mathbf{x}}\|} \,\mathrm{d}\vec{\mathbf{y}} + \int_{\Gamma_{2,i}} \frac{f(\vec{\mathbf{x}})}{\|\vec{\mathbf{y}} - \vec{\mathbf{x}}\|} \,\mathrm{d}\vec{\mathbf{y}} \\ &= \int_{\Gamma_{2,i}} \frac{f(\vec{\mathbf{y}}) - f(\vec{\mathbf{x}})}{\|\vec{\mathbf{y}} - \vec{\mathbf{x}}\|} \,\mathrm{d}\vec{\mathbf{y}} + f(\vec{\mathbf{x}}) \int_{\Gamma_{2,i}} \frac{1}{\|\vec{\mathbf{y}} - \vec{\mathbf{x}}\|} \,\mathrm{d}\vec{\mathbf{y}}\,. \end{aligned} \tag{4.77}$$

The second integral needs to be solved analytically. Writing out the norm, we obtain

$$\int_{\Gamma_{2,i}} \frac{1}{\|\vec{\mathbf{y}} - \vec{\mathbf{x}}\|} \, \mathrm{d}\vec{\mathbf{y}} = \int_{\Gamma_{2,i}} \frac{1}{\sqrt{(y_1 - x_1)^2 + (y_2 - x_2)^2 + (y_3 - x_3)^2}} \, \mathrm{d}\vec{\mathbf{y}} \,. \tag{4.78}$$

Here, we denote $\vec{\mathbf{x}} = (x_1, x_2, x_3)^T$ and similarly we denote $\vec{\mathbf{y}}$. When we use the fact that we only need to treat the singularity if the evaluation point $\vec{\mathbf{x}}$ lies on the cuboid's boundary, i.e. at least one of the coordinates are equal, this integral reduces to

$$\int_{\Gamma_{2,i}} \frac{1}{\|\vec{\mathbf{y}} - \vec{\mathbf{x}}\|} \, \mathrm{d}\vec{\mathbf{y}} = \int_{\Gamma_{2,i}} \frac{1}{\sqrt{(y_1 - x_1)^2 + (y_2 - x_2)^2}} \, \mathrm{d}\vec{\mathbf{y}} \,. \tag{4.79}$$

W.l.o.g. we have assumed that $x_3 = y_3$. Now, the second integral can be computed analytically, e.g. using Mathematica [26],

$$\begin{aligned} \int_{\Gamma_{2,i}} \frac{1}{\|\vec{\mathbf{y}} - \vec{\mathbf{x}}\|} \, \mathrm{d}\vec{\mathbf{y}} &= -y_2 \\ &+ (y_2 - x_2) \log\left(\sqrt{y_1^2 - 2y_1x_1 + y_2^2 - 2y_2x_2 + x_1^2 + x_2^2} + y_1 - x_1\right) \\ &+ (y_1 - x_1) \log\left(\sqrt{y_1^2 - 2y_1x_1 + y_2^2 - 2y_2x_2 + x_1^2 + x_2^2} + y_2 - x_2\right) \Big|_{\underline{y}_1}^{\overline{y}_1} \Big|_{\underline{y}_2}^{\overline{y}_2}, \end{aligned} \tag{4.80}$$

where $\underline{y}_1$ and $\overline{y}_1$ denote the integral limits of y_1 and the limits for y_2 are represented analogously. The first integral in Eq. (4.77) is evaluated using a usual Gaussian quadrature rule, i.e.

$$\int_{\Gamma_{2,i}} \frac{f(\vec{\mathbf{y}}) - f(\vec{\mathbf{x}})}{\|\vec{\mathbf{y}} - \vec{\mathbf{x}}\|} \, \mathrm{d}\vec{\mathbf{y}} \approx \sum_{i=1}^{N} \sum_{j=1}^{M} w_{ij} \frac{f(\vec{\mathbf{y}}_{ij}) - f(\vec{\mathbf{x}})}{\|\vec{\mathbf{y}}_{ij} - \vec{\mathbf{x}}\|}. \tag{4.81}$$

Here, w_{ij} and $\vec{\mathbf{y}}_{ij}$ are the tensorized Gauß-Legendre quadrature weights and points on the cuboid's face, respectively. If $\vec{\mathbf{y}}_{ij} = \vec{\mathbf{x}}$, we substitute

$$\frac{f(\vec{\mathbf{y}}_{ij}) - f(\vec{\mathbf{x}})}{\|\vec{\mathbf{y}}_{ij} - \vec{\mathbf{x}}\|} = 0 \tag{4.82}$$

using the rule of l'Hôpital.

Table 1. Details of the Computer

Description	Value	Unit
Memory Size	8	[GiB]
Memory Clocking	1600	[MHz]
Processor Type	Intel® Core™ i5–3230M	
Processor Clocking	2.60	[GHz]
OS	Linux	

Table 2. Set-Up Interior Dirichlet Problem in a Cube

Description	Quantity	Value
Width	x	$[-1, 1]$
Depth	y	$[-1, 1]$
Height	z	$[0, 2]$
Collocation Points per Dimension	N	$[1, 20]$
CGS Tolerance	`tol`	1×10^{-6}

5. Numerical Results

We are interested in the relative errors as well as run times w.r.t. degrees of freedom and number of quadrature points. First, we present the results for the four different solvers. Then we show a test case that combines all the solvers into a scalar magnetic potential (SMP) solver.

All the computations were conducted on a machine with the settings displayed in Table 1. The results are averaged over 10 runs. Let u denote an exact solution and $\tilde{u}$ its approximation. The relative error reads

$$e_{\text{rel}} = \frac{\|u - \tilde{u}\|}{\|u\|}, \tag{5.1}$$

with $\|\cdot\|$ being either the L^1-, L^2-, or L^∞-norm. If the exact solution could not be provided, we compare the approximation to another approximation with finer resolution.

5.1. Interior Dirichlet Problem in a Cube.

In this constructed example we are looking at a cube $\Omega_{\text{mag}} \coloneqq [-1, 1] \times [-1, 1] \times [0, 2]$ with boundary $\Gamma_{\text{mag}} = \partial\Omega_{\text{mag}}$. In the cube, the Poisson problem

$$\begin{aligned} \Delta v_{\text{int}} &= f, \quad \text{in} \quad \Omega_{\text{mag}} \\ v_{\text{int}} &= 0, \quad \text{on} \quad \Gamma_{\text{mag}}. \end{aligned} \tag{5.2}$$

is solved. The Poisson data is given by

$$f(x, y, z) = -1200\pi^2 \sin(2\pi x) \sin(2\pi y) \sin(2\pi z), \tag{5.3}$$

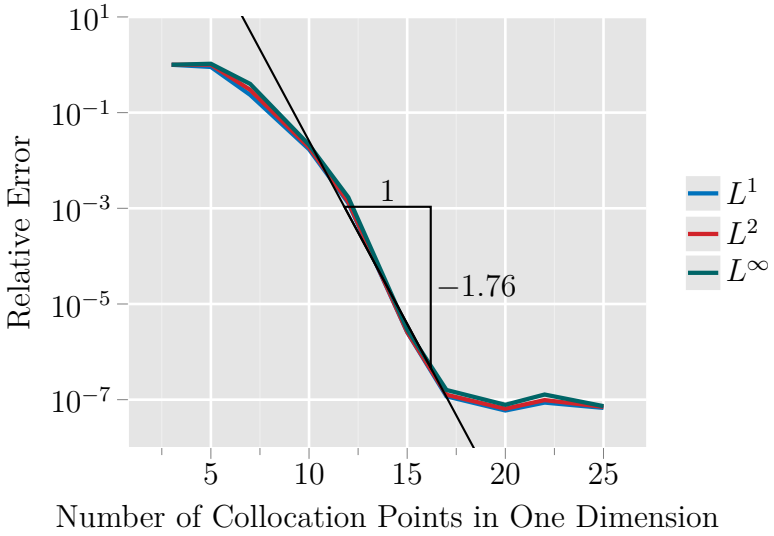

Figure 8. Error in Solution.

such that the exact solution reads

$$v_{\text{int, exact}}(x, y, z) = 100 \sin(2\pi x) \sin(2\pi y) \sin(2\pi z). \tag{5.4}$$

Since we are also interested in the derivative in direction to the outward pointing unit normal, the gradient is computed. The exact gradient reads

$$\boldsymbol{\nabla} v_{\text{int, exact}} = \begin{pmatrix} 200\pi \cos(2\pi x) \sin(2\pi y) \sin(2\pi z) \\ 200\pi \sin(2\pi x) \cos(2\pi y) \sin(2\pi z) \\ 200\pi \sin(2\pi y) \sin(2\pi x) \cos(2\pi z) \end{pmatrix}. \tag{5.5}$$

We increase the number of collocation points used in the spectral collocation method from 1 to 20 and look at the error as well as the run times.

In Fig. 8 we see exponential convergence in the solution w.r.t. the number of collocation points. Same holds for the computation of the gradient, as can be seen in Fig. 9. The run time grows exponentially w.r.t. the number of collocation points (see Fig. 10).

The convergence rate in the collocation method is exactly as expected and shows the algorithm's advantages over, e.g., the finite element method. The runtime of *Matlab*'s `cgs` solver grows with a factor of $N^{4.4}$, but most of the time in the collocation method is spent assembling the system matrix and computing the interpolation's coefficients. Latter could be implemented more efficiently by exploiting the Chebyshev polynomial's multiplication rules. Now if we look at Fig. 11, the number of iterations until convergence of the `cgs` solver is linearly correlated with the number of collocation points. Additionally, it requires less iteration than the size of the matrix.

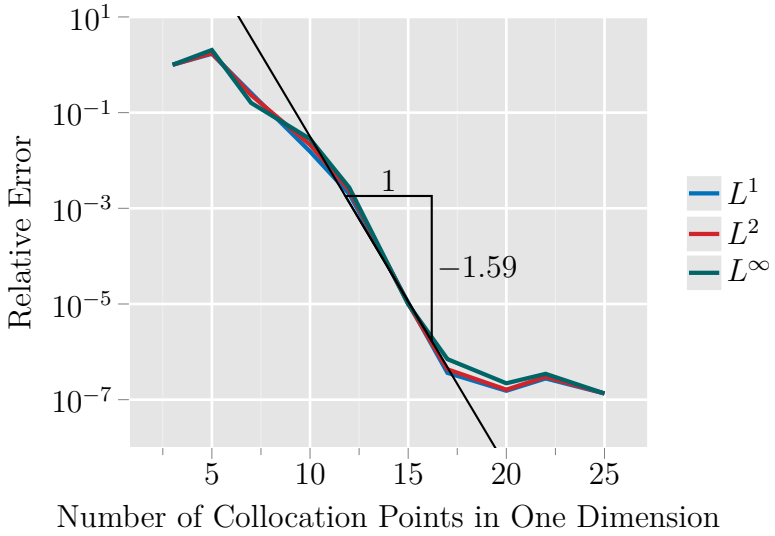

Figure 9. Error in Derivative.

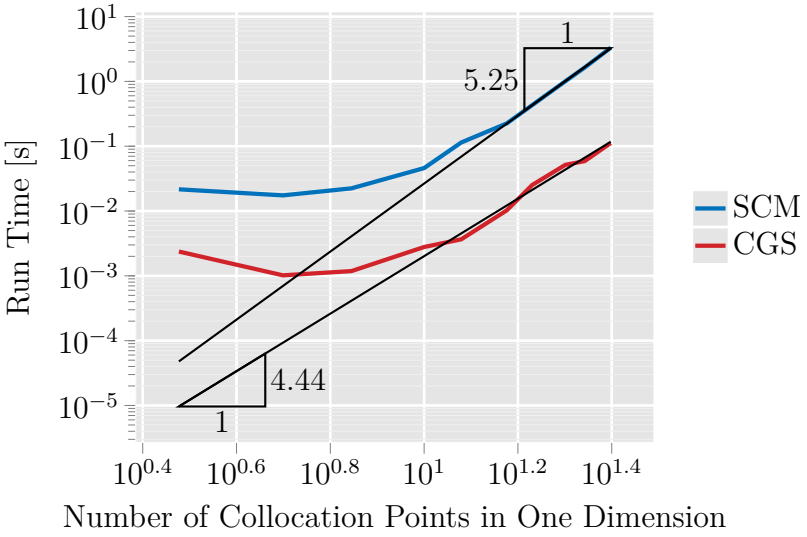

Figure 10. Run Time of the complete Spectral Collocation Method (SCM) and *Matlab*'s `cgs` Solver (CGS).

Now we set the exact solution to Eq. (3.6) to

$$v_{\text{int, exact}}(x, y, z) = \sin(2\pi a x)\sin(2\pi a y)\sin(2\pi a z). \tag{5.6}$$

Therefore, the right-hand side reads

$$f(x, y, z) = -12\pi^2 a^2 \sin(2\pi a x)\sin(2\pi a y)\sin(2\pi a z). \tag{5.7}$$

In Fig. 12 we can observe that the oscillation of the solution is related to the number of collocation points in the following way. The higher the oscillation rate, the more points are needed to represent the solution. One can also see, that if we double the wave number k we do not need to double the number of collocation points. However, this observation

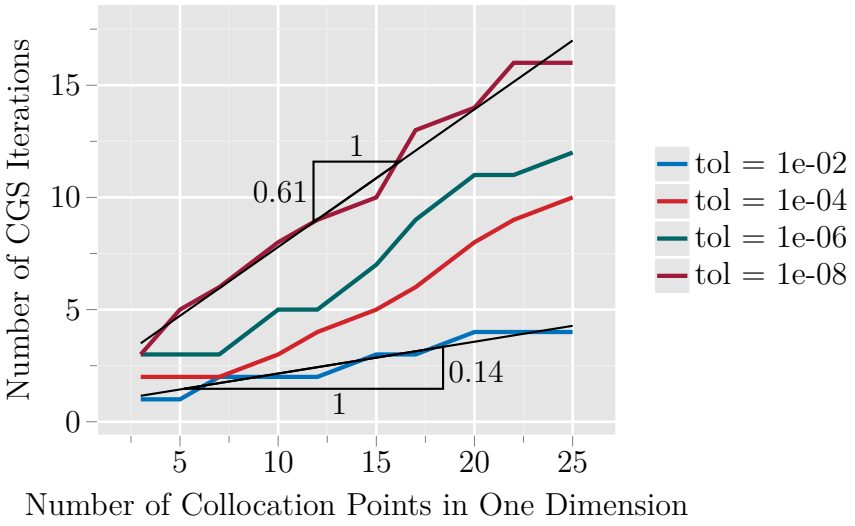

Figure 11. Iterations of the CGS Solver.

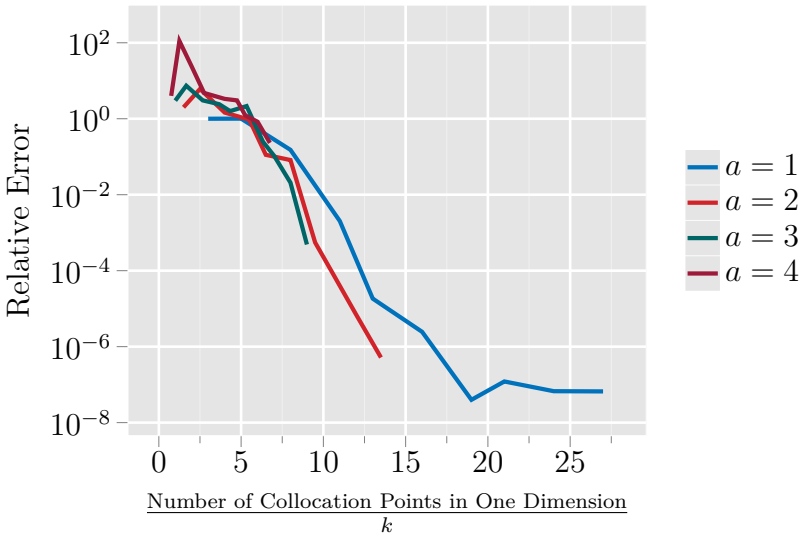

Figure 12. Error in Parameterized Solution.

is only really clear for $k = 1$ and $k = 2$. The trend continues for $k = 3$, but it would be preferable to validate this statement for higher wave numbers as well.

5.2. **Homogeneously Magnetized Cube.** We are now analysing the quadrature rule in the single layer potential computation for the unit cube $(x, y, z) \in [-0.5, 0.5] \times [-0.5, 0.5] \times [0, 1]$. The cube is homogeneously magnetized $\vec{\mathbf{M}}_2 = (0, 0, 1)^T$, effectively shutting off the solver for the Eq. (3.6), since $\boldsymbol{\nabla}\vec{\mathbf{M}}_2 = 0$. In Table 3 the initial values are shown. We evaluate the scalar magnetic potential generated by the cube at 30 points $\vec{\mathbf{p}} = (0, 0, -3.1)^T, \ldots, (0, 0, 3.1)^T$. Since the exact solution is not known, a reference solution is computed with 40 quadrature points.

Table 3. Set-Up Homogeneously Magnetized Unit Cube

Description	Quantity	Value
Width	x	$[-0.5, 0.5]$
Depth	y	$[-0.5, 0.5]$
Height	z	$[0, 1]$
Magnetization	$\vec{\mathbf{M}}$	$(0, 0, 1)^T$
Poisson Data	f	0
Neumann BC	g	$\vec{\mathbf{M}} \cdot \vec{\mathbf{n}}$
Gaussian Quadrature Points	N	$[1, 30]$

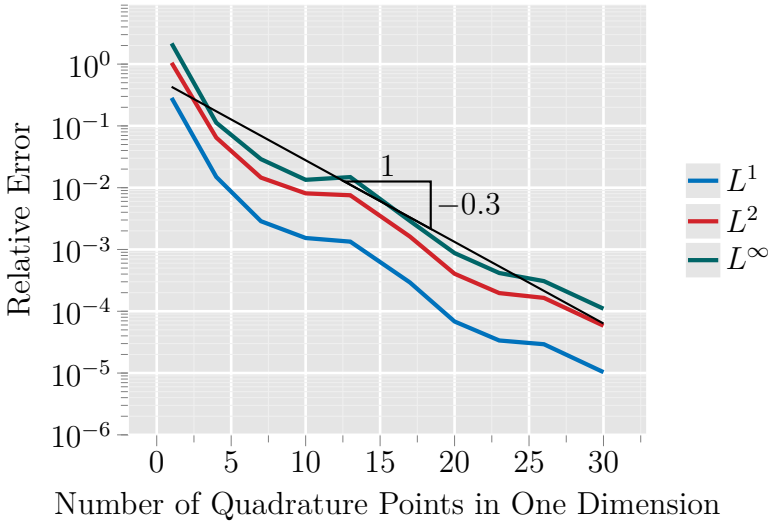

Figure 13. Error w.r.t. Number of Quadrature Points.

In Fig. 13 a exponential convergence rate is observed. However, as can be seen in Figs. 15–17, the convergence rate gets slower the closer we evaluate the potential at the boundary. In Fig. 14 we again see slightly more than quadratic growth in the run time w.r.t. the number of quadrature points.

The run times are again as expected. The interesting part, however, is the bad convergence rate we see when evaluating near a boundary. In literature this is a known problem [see, e.g., 15] and a lot of modified quadrature rules are developed in order to overcome this scenario [see, e.g., 11, 15, 22].

5.3. **Inhomogeneously Magnetized Sphere.** In this example we have implemented a test case from Kaliche [14], namely, the inhomogeneously magnetized sphere. In Table 4 the geometry, the right-hand sides, and the boundary conditions are stated. The exact solution as well as the solver defaults are shown in Listing 1. Since Kaliche [14] provides an exact solution, we can validate the solver for the spheres.

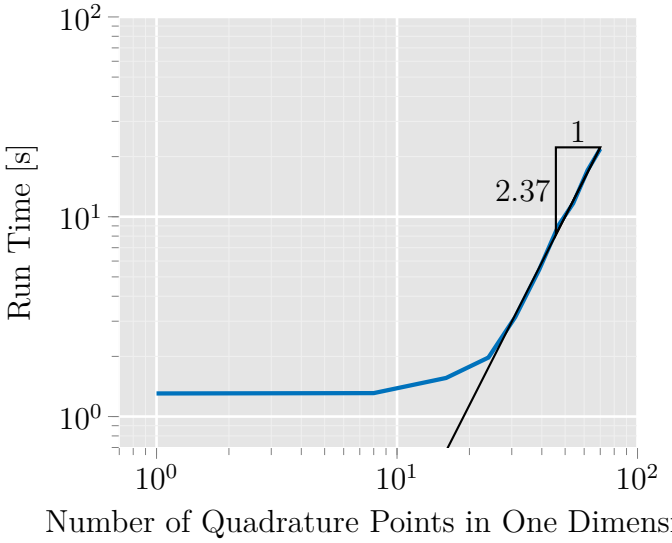

Figure 14. Run Time w.r.t. Number of Quadrature Points.

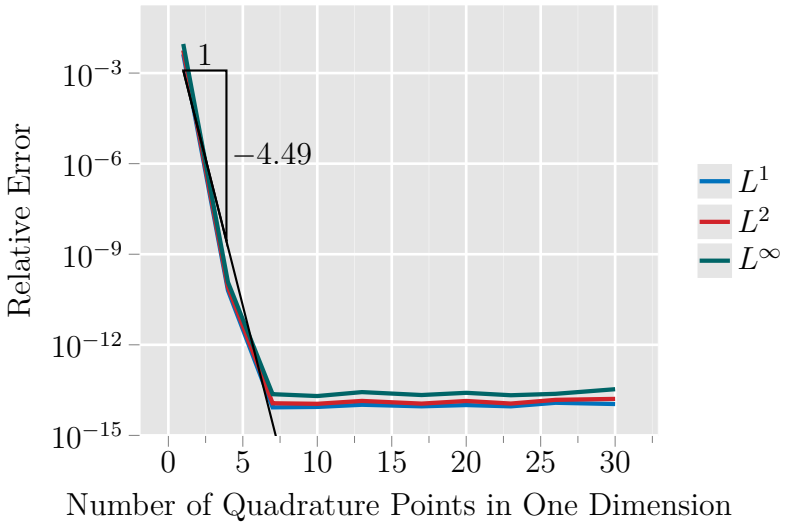

Figure 15. Error w.r.t. Number of Quadrature Points (Far).

First, we increase the number of radial quadrature points while the order of the Lebedev quadrature rule is fixed at 23. We then increase the quadrature rule's order from 3 to 23 for the angles while fixing the number of radial quadrature points at 60.

As can be seen in Fig. 18, the convergence rate is linear. In Fig. 19 it can be observed, that the Lebedev quadrature evaluates an integral over the sphere's surface exactly for 11 quadrature points. First, the Lebedev quadrature error dominates, then the quadrature rule evaluates the integral exactly, but now the radial error dominates and increasing the number of Lebedev points cannot increase the precision.

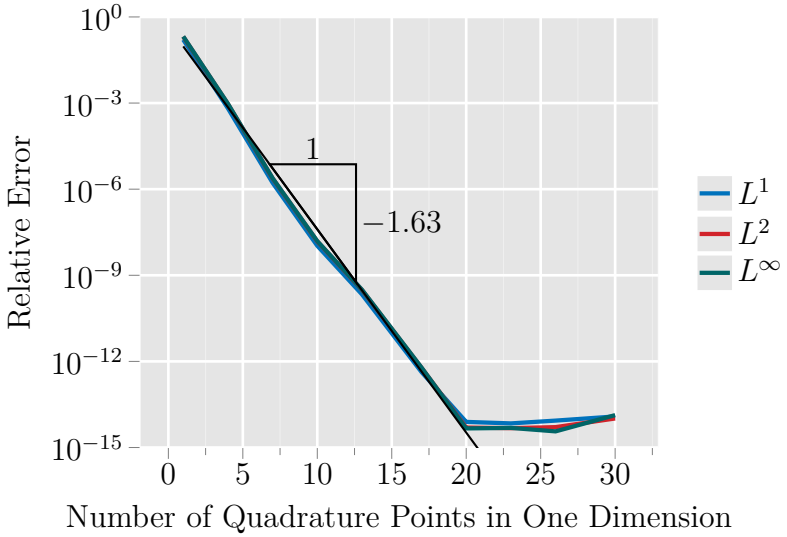

Figure 16. Error w.r.t. Number of Quadrature Points (Near).

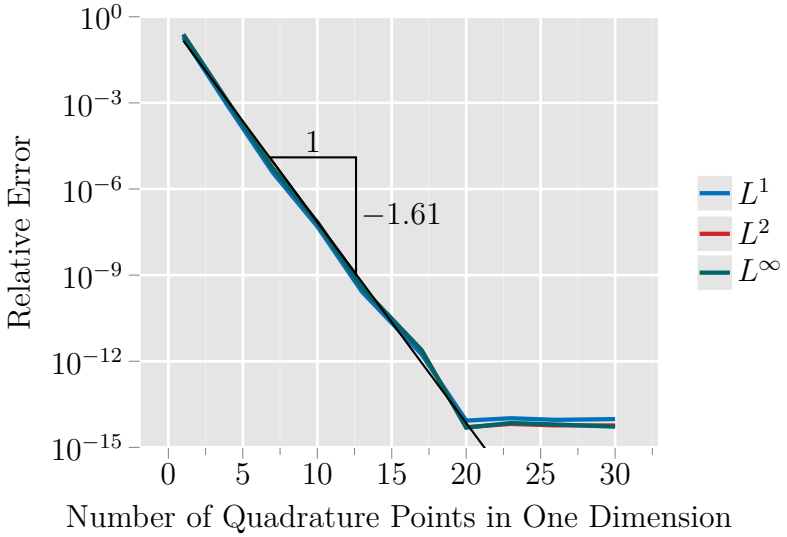

Figure 17. Error w.r.t. Number of Quadrature Points (On).

5.3.1. *Parallelization of the Interior Dirichlet Solver.* The mathematical setting in this example is the same as in Section 5.3. The geometric set-up, however, is different. Since we want to look at the scaling w.r.t. the number of spheres, we read the values for the centers and radii of non-overlapping spheres from a file (see Listing 2). The radial number of quadrature points is fixed to 10, the spherical harmonics series is truncated at 5. We consider up to 1000 spheres and compare *Matlab*'s `for`-loop with *Matlab*'s `parfor`-loop. The `parpool` consists of 2 workers.

In Fig. 20 we can see good parallelization.

Table 4. Set-Up Inhomogeneously Magnetized Sphere

Description	Quantity	Value
Radius	R	0.5
Center	c	$(0,0,0)^T$
Magnetization	$\vec{\mathbf{M}}$	$(\sin(\theta),\cos(\theta),0)^T$
Poisson Data	f	$2\cos\theta/r$
Neumann BC	g	0
Spherical Harmonics Truncation	$\ell_{\max}$	5
Radial Discretization	M	60
Lebedev Quadrature Orders	O	$\{3,5,\ldots,23\}$

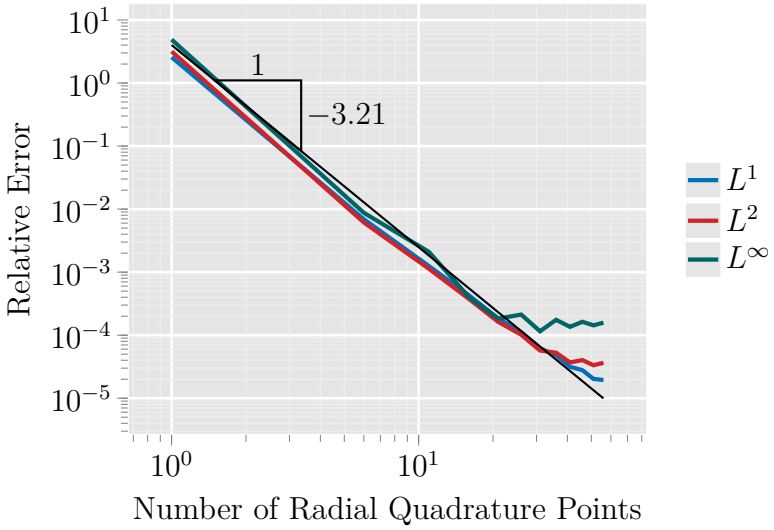

Figure 18. Error w.r.t. Radial Quadrature Points.

Figure 19. Error w.r.t. Order of Lebedev Quadrature.

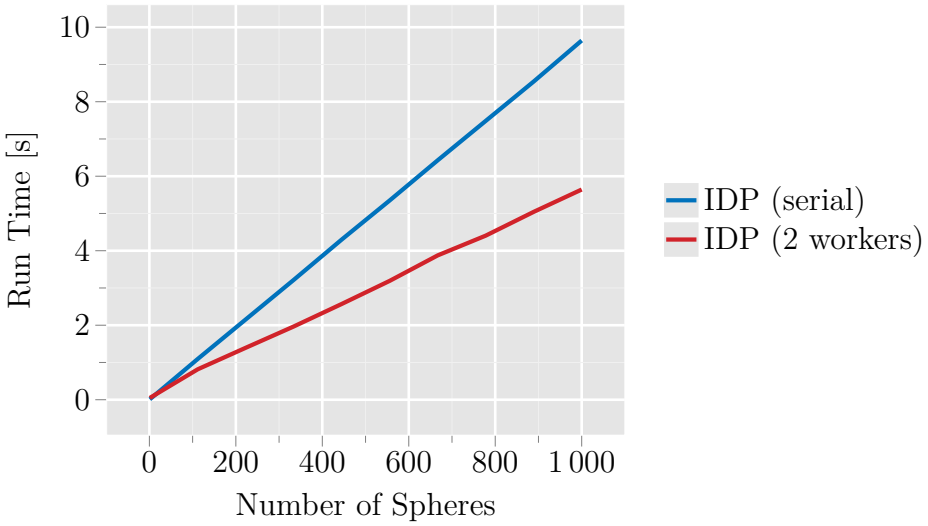

Figure 20. Run Time w.r.t. Number of Spheres. The serial and parallel versions of the interior Dirichlet problem (IDP) solver of Eq. (3.8) has been timed. For the parallelization, *Matlab*'s `parfor`-loop construct was used and a parallel pool of 2 workers has been set up. This corresponds to running the code on 2 CPU cores.

Since the problem is completely separated, this is exactly what we expected. The overhead is the usual copying and communications overhead.

5.3.2. *Run Time of the Fast Multipole Method.* In this test case, we look at the run time behavior of the fast multipole method (FMM) w.r.t. the number of spheres. The set-up is equal to the one in Section 5.3.1. Except that we now evaluate the potential at $\vec{\mathbf{p}} = (-4, 0, 0)^T, \ldots, (4, 0, 0)^T$. First, the number of spheres is increased and the potential is evaluated at just one point. Then, the number of spheres is set to 1000 and the number of query points is increased from 0 to 1000. Last but not least, we increase both, the number of spheres and the number of evaluation points, at the same rate and at the same time.

In Fig. 21 we see a linear behavior of the run time w.r.t. the number of spheres. The plot int Fig. 22 shows a slight increase in computation time while increasing the number of evaluation points up to 1000. Increasing the number of spheres and the number of query points at the same time also shows a linear increase in run time (see Fig. 23).

In essence, this behavior is as expected, because the FMM speeds up the computation of N spheres at M query points from $\mathcal{O}(NM)$ to $\mathcal{O}(N)$.

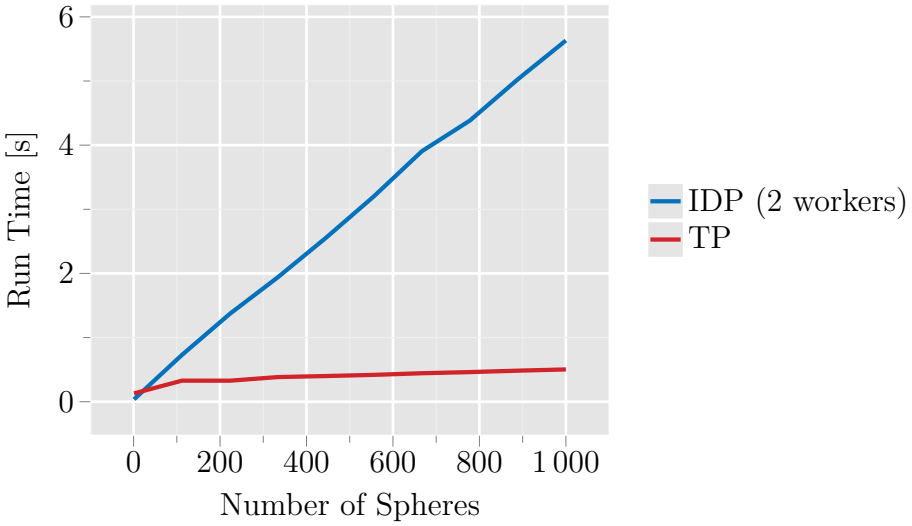

Figure 21. Run Time w.r.t. Number of Spheres. Here, the interior Dirichlet problem (IDP) solver of Eq. (3.8) as well as the transmission problem (TP) solver for Eq. (3.9) is shown. The number of spheres is increased and the number of evaluation points is fixed at 1.

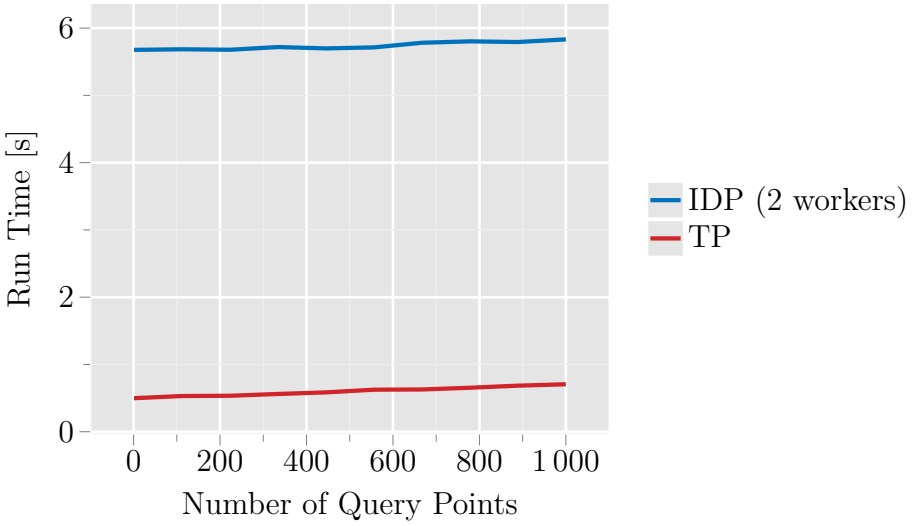

Figure 22. Run Time w.r.t. Number of Query Points. Again, the solvers for the interior Dirichlet problem (IDP) and the transmission problem (TP) are displayed, but now the number of evaluation points is increased while holding the number of spheres fixed at 1000.

5.4. **Scalar Magnetic Potential of a Magnonic Crystal.** Hitherto, we have analysed the four subproblems in the scalar magnetic potential solver.

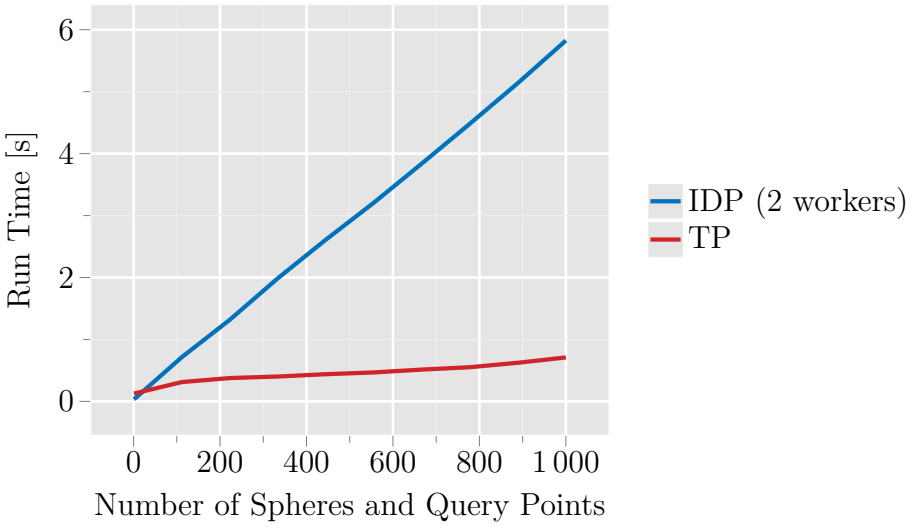

Figure 23. Run Time w.r.t. Number of Spheres and Query Points. This time, both the number of points and the number of spheres are increased simultaneously and the transmission problem (TP) and the interior Dirichlet problem (IDP) solvers are compared.

Table 5. Set-Up Homogeneously Magnetized Magnonic Crystal

Description	Quantity	Value
Dimension of the Cube	(x, y, z)	$[-50, 50]^3$
Cut through the Cube	y	5
Radius of Spheres	R	`2*rand(1000)`
Sphere Center Generator	`x`	`linspace(-45,45,10)`
Centers	$\vec{\mathbf{c}}$	`meshgrid(x,x,x)`
Radius of Zoomed-In Sphere	R'	1.5
Center of Zoomed-In Sphere	$\vec{\mathbf{c}}'$	$(5, 5, 5)$
Spherical Harmonics Truncation	$\ell_{\max}$	5
Spectral Collocation Points	N	15
Radial Discretization	M	10

5.4.1. *Homogeneously Magnetized Magnonic Crystal.* Now, we set up a more realistic test case and present the results. The geometrical set-up is described in Table 5. We present three different settings w.r.t. the magnetization: (1) The spheres' magnetization is stronger than the cube's magnetization. (2) Both magnetizations are equal. (3) The cube's magnetization is stronger than the spheres' magnetization. Notice, that the following results are not averaged over 10 runs.

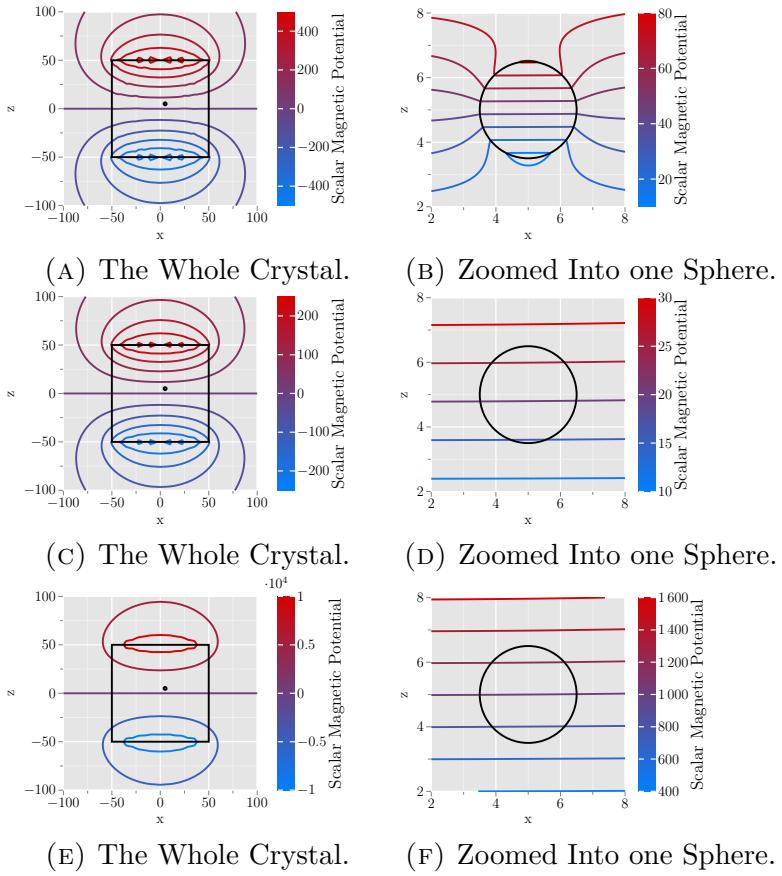

(A) The Whole Crystal. (B) Zoomed Into one Sphere.

(C) The Whole Crystal. (D) Zoomed Into one Sphere.

(E) The Whole Crystal. (F) Zoomed Into one Sphere.

Figure 24. Homogeneously Magnetized Magnonic Crystal. In the left column a cut through the crystal is visualized. The right column shows a magnification of one of the embedded spheres, that can be seen in the left plot. From top to bottom the magnetization of the cube and the spheres changes. In the top row, the spheres' magnetization is larger than the cube's one. The row in the middle visualizes an equal magnetization of the cube and the spherical inclusions. The last row pictures a crystal in which the spheres are less magnetized than the cube.

In the first case, the cube's magnetization is set to $\vec{\mathbf{M}}_2(x, y, z) = (0, 0, 2)^T$. Therefore, the Poisson data is $f(x, y, z) = 0$ and the Neumann boundary is $g(x, y, z) = \vec{\mathbf{M}}_2(x, y, z) \cdot \vec{\mathbf{n}}(x, y, z)$. The spheres are magnetized with $\vec{\mathbf{M}}_1(x, y, z) = (0, 0, 48)^T$. The Poisson data for the sphere is therefore $f(r, \theta, \varphi) = 0$ and the Neumann boundary reads $g(r, \theta, \varphi) = 50r \cos\theta$.

In Fig. 24a the scalar magnetic potential is shown. It is quite homogeneous on the outside of the cube, but exhibits perturbations inside

Table 6. Set-Up Inhomogeneously Magnetized Magnonic Crystal

Description	Quantity	Value
Dimension of the Cube	(x, y, z)	$[-50, 50]^3$
Cut through the Cube	y	5
Radius of Spheres	R	`2*rand(1000)`
Sphere Center Generator	`x`	`linspace(-45,45,10)`
Centers	$\vec{\mathbf{c}}$	`meshgrid(x,x,x)`
Radius of Zoomed-In Sphere	R'	1.5
Center of Zoomed-In Sphere	$\vec{\mathbf{c}}'$	$(5, 5, 5)$
Spherical Harmonics Truncation	$\ell_{\max}$	10
Spectral Collocation Points	N	15
Radial Discretization	M	10

the cube. In Fig. 24b a spherical inclusion is displayed in more detailed. Here we can see the distortions of the equipotential lines.

The distortions in the equipotential lines are generated by the spheres which can be observed in the zoomed-in plot. The asymmetry in the spherical inclusion's potential is due to the positioning w.r.t. the cube.

Now if we set both potentials equal, i.e. $\vec{\mathbf{M}}_1 = \vec{\mathbf{M}}_2 = (0, 0, 1)^T$, the Poisson data and Neumann boundary of Eqs. (3.8) and (3.9) vanish.

It can be observed in Figs. 24c and 24d that the spheres don't interact with the cube's magnetization.

Since in the equations for the spherical domain the right-hand sides are zero, no data can be generated by the solver. This makes sense, both mathematically and physically, because we are basically looking at a magnetic cube without spherical inclusions.

In our last test case we set the cube's magnetization to $\vec{\mathbf{M}}_2 = (0, 0, 48)$ and the spheres' magnetization to $(0, 0, 2)$. Therefore, we get for the spheres' Poisson data $f = 0$ and for the Neumann boundary $g(r, \theta, \varphi) = 2r \cos\theta$.

The results in Figs. 24e and 24f look similar to the results in Figs. 24c and 24d. However, the potential is two magnitudes higher. Since magnetism is a very strong force, the spherical inclusions just don't have a significant contribution to the cube's potential.

5.4.2. *Inhomogeneously Magnetized Magnonic Crystal.* This test case is designed such that every solver contributes to the overall simulation. The setup is shown in Table 6. We define the cube's magnetization to be $\vec{\mathbf{M}}_2 = (\sin\theta, \cos\theta, 0)^T$ and the sphere's magnetization to $\vec{\mathbf{M}}_1 = (0, 0, 0)^T$. For the two problems describing the cubic domain, this yields

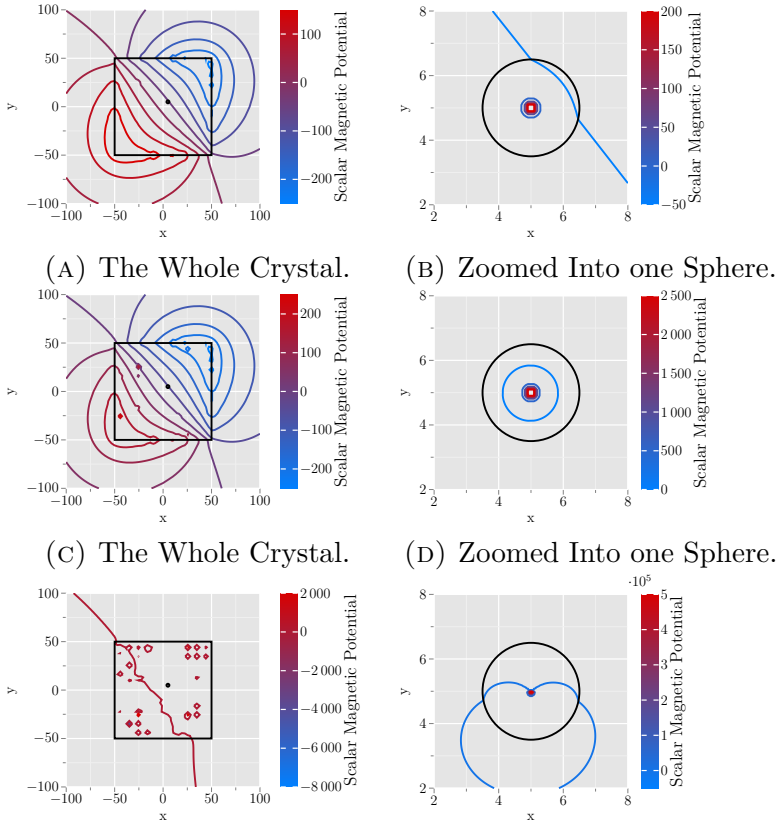

(A) The Whole Crystal. (B) Zoomed Into one Sphere.

(C) The Whole Crystal. (D) Zoomed Into one Sphere.

(E) The Whole Crystal. (F) Zoomed Into one Sphere.

Figure 25. Inhomogeneously Magnetized Magnonic Crystal. Again in the left column a cut through the magnonic crystal is visualized and in the right column, it is zoomed into a sphere. From top to bottom, the magnetization is successively increased.

the Poisson data

$$f(x,y,z) = \frac{xz^2}{\sqrt{\frac{x^2}{x^2+y^2+z^2} + \frac{y^2}{x^2+y^2+z^2}}\left(x^2+y^2+z^2\right)^2} - \frac{yz}{\left(x^2+y^2+z^2\right)^{\frac{3}{2}}}$$

and the Neumann boundary data $g = -\left(\vec{\mathbf{M}}_2 \cdot \vec{\mathbf{n}}\right)$. And the Neumann boundary data for the spherical inclusions then reads $g = 0$. The Poisson data of the spherical inclusions is first set to $f = \frac{20\cos\theta}{r}$, then increased to $f = \frac{200\cos\theta}{r}$ and in a last step defined as $f = \frac{2000\cos\theta}{r}$.

In Figs. 25a–25f it can be seen, that the higher the difference in the magnetization of the spherical inclusions w.r.t. the cubic carrier material, the more artifacts arise in the scalar magnetic potential.

6. Conclusion

Micromagnetic simulations are an important tool in the study of magnonic crystals and their applications. The simulations are time-consuming, but at the same time it is of great interest to look at longer time scales and with high accuracy. Obviously, this contradicts the time-consuming nature of those simulations. The need for efficient and accurate algorithms is therefore natural.

In this Thesis, such an algorithm has been developed for the computation of the scalar magnetic potential (SMP) of multiple spheres embedded in a cubic carrier material. After stating the mathematical description of such a magnonic crystal, the transmission problem has been decoupled into two subproblems describing the spherical inclusions and two subproblems describing the cubic domain. For these problems, the variational formulation have been derived and their well-posedness have been stated. A spectral collocation method was implemented and a single layer potential was solved in order to describe the SMP of the cuboid. For the spherical inclusions, the properties of the spherical harmonics were exploited and the fast multipole method (FMM) has been incorporated.

The resulting SMP solver shows promising accuracy and efficiency. The potential of a magnonic crystal consisting of 1000 spherical inclusions could be computed within 4 s. However, at the time of writing, it is assumed that the evaluation points do not lie at one of the spheres' centers. It has been shown that the computation of the Eq. (3.8) for multiple spheres could be accelerated using more CPU cores. The solver for Eq. (3.6) should be reconsidered, though. With the currently implemented spectral collocation method a lot of time is spent computing the discrete Laplace operator using the Kronecker tensor product and the interpolation coefficients and can be avoided.

In future research, a spectral Galerkin method could be implemented, which directly computes the coefficients of an expansion in basis functions and therefore, the interpolation would be obsolete. Another possibility would be the incorporation of the Kronecker delta product into the solver of the linear system. This would also reduce the amount of memory tremendously. Since in the current implementation of the FMM the evaluation of the potential within a source region is not considered, a correction term was added to yield a correct solution. This is both time consuming and unnecessary from a mathematical point of view. It is therefore of interest to incorporate the evaluation within source regions into the FMM algorithm. Finally, the comparison to other existing solvers would be beneficial. One could either write a complete Landau-Lifshitz-Gilbert (LLG) solver or incorporate the SMP solver in an existing micromagnetic simulation in order to compare the algorithm to other methods.

References

[1] C. W. Abert. "Discrete Mathematical Concepts in Micromagnetic Computations". PhD thesis. Hamburg: Staats- und Universitätsbibliothek Hamburg, Nov. 14, 2013. URL: http://ediss.sub.uni-hamburg.de/volltexte/2013/6458 (cit. on pp. 2, 4–6, 9).

[2] F. S. Acton. *Numerical methods that work*. Washington, D.C: Mathematical Association of America, 1990. 549 pp. ISBN: 978-0-88385-450-1 (cit. on p. 31).

[3] C. H. Back. "Minimum Field Strength in Precessional Magnetization Reversal". In: *Science* 285.5429 (Aug. 6, 1999), pp. 864–867. ISSN: 00368075, 10959203. DOI: 10.1126/science.285.5429.864. URL: http://www.sciencemag.org/cgi/doi/10.1126/science.285.5429.864 (visited on 08/29/2017) (cit. on p. 4).

[4] C. Bauer and B. Stamm. "Computing the Scalar Magnetic Potential using Spherical Harmonics". CES Seminar Report. RWTH Aachen University, 2017 (cit. on p. 1).

[5] R. Beatson and L. Greengard. "A short course on fast multipole methods". In: *Wavelets, multilevel methods, and elliptic PDEs*. Oxford University Press, 1997. URL: https://nyu.pure.elsevier.com/en/publications/a-short-course-on-fast-multipole-methods (cit. on pp. 21, VII–IX).

[6] P. Blanchard et al. "ScalFMM: A Generic Parallel Fast Multipole Library". In: SIAM Conference on Computational Science and Engineering (SIAM CSE 2015). Mar. 14, 2015. URL: https://hal.inria.fr/hal-01135253 (visited on 11/05/2017) (cit. on p. 29).

[7] M. Bolte et al. "Simulation of micromagnetic phenomena". In: *Proceedings of the 18th European Simulation Conference*. 2004, pp. 407–412. URL: http://scs-europe.net/services/esm2004/pdf/esm-63.pdf (visited on 06/21/2016) (cit. on pp. 1, 3, 5, 6, 8).

[8] R. Feynman, R. Leighton, and M. Sands. *The Feynman Lectures on Physics, Volume II*. 2013. URL: http://feynmanlectures.caltech.edu/II_toc.html (visited on 05/17/2017) (cit. on p. 7).

[9] C. J. García-Cervera, Z. Gimbutas, and E. Weinan. "Accurate numerical methods for micromagnetics simulations with general geometries". In: *Journal of Computational Physics* 184.1 (2003), pp. 37–52. URL: http://www.sciencedirect.com/science/article/pii/S0021999102000141 (visited on 05/17/2016) (cit. on pp. 4, 5).

[10] L. Greengard and V. Rokhlin. "A Fast Algorithm for Particle Simulations". In: *J. Comput. Phys.* 73.2 (Dec. 1987), pp. 325–348. ISSN: 0021-9991. DOI: 10.1016/0021-9991(87)90140-9. URL:

http://dx.doi.org/10.1016/0021-9991(87)90140-9 (visited on 05/24/2017) (cit. on pp. 29, X).

[11] Y. Gu et al. "A general algorithm for evaluating nearly strong-singular (and beyond) integrals in three-dimensional boundary element analysis". In: *Computational Mechanics* 59.5 (May 1, 2017), pp. 779–793. ISSN: 0178-7675, 1432-0924. DOI: 10.1007/s00466-016-1372-1. URL: https://link.springer.com/article/10.1007/s00466-016-1372-1 (visited on 11/14/2017) (cit. on p. 37).

[12] R. Huber. "Control of Spin Waves on the Nanoscale in One-Dimensional Magnonic Crystals and Atomic Layer Deposition of Metallic Ferromagnets for Second Generation of Nanomaterials". PhD thesis. München: Technische Universität München, Dec. 6, 2013 (cit. on pp. 5, 6).

[13] D. Jiles. *Introduction to magnetism and magnetic materials*. Third edition. OCLC: ocn909323904. Boca Raton: CRC Press, Taylor & Francis Group, 2016. 588 pp. ISBN: 978-1-4822-3887-7 (cit. on pp. 2–4, 6, 7).

[14] K. Kaliche. "Méthode des éléments finis inversés pour des domaines non bornés". PhD thesis. Paris Saclay, 2016. URL: http://www.theses.fr/2016SACLV014 (visited on 05/17/2016) (cit. on pp. 6, 37).

[15] P. Kolm and V. Rokhlin. "Numerical quadratures for singular and hypersingular integrals". In: *Computers & Mathematics with Applications* 41.3 (Feb. 1, 2001), pp. 327–352. ISSN: 0898-1221. DOI: 10.1016/S0898-1221(00)00277-7 (cit. on p. 37).

[16] M. Krawczyk and D. Grundler. "Review and prospects of magnonic crystals and devices with reprogrammable band structure". In: *Journal of Physics: Condensed Matter* 26.12 (2014), p. 123202. ISSN: 0953-8984. DOI: 10.1088/0953-8984/26/12/123202. URL: http://stacks.iop.org/0953-8984/26/i=12/a=123202 (visited on 10/31/2016) (cit. on p. 2).

[17] U. Langer, ed. *Fast Boundary Element Methods in Engineering and Industrial Applications*. Lecture Notes in Applied and Computational Mechanics Volume 63. Heidelberg: Springer, 2012. 269 pp. ISBN: 978-3-642-25669-1 (cit. on p. 8).

[18] V. Lebedev and D. Laikov. "A quadrature formula for the sphere of the 131st algebraic order of accuracy". In: Doklady. Mathematics. Vol. 59. MAIK Nauka/Interperiodica, 1999, pp. 477–481 (cit. on p. 27).

[19] A. Maksymov and L. Spinu. "Static and dynamic properties of three-dimensional dot-type magnonic crystals". In: *Physica B: Condensed Matter*. 10th International Symposium on Hysteresis Modeling and Micromagnetics (HMM 2015) 486 (Apr. 1, 2016), pp. 177–182. ISSN: 0921-4526. DOI: 10.1016/j.physb.2015.10.

032. URL: http://www.sciencedirect.com/science/article/pii/S0921452615302982 (cit. on p. 1).

[20] J. C. Mason and D. C. Handscomb. *Chebyshev polynomials*. Boca Raton, Fla: Chapman & Hall/CRC, 2003. 341 pp. ISBN: 978-0-8493-0355-5 (cit. on pp. 21, 22, 29).

[21] C. Quan, B. Stamm, and Y. Maday. "Generalized ddPCM Method for the SES-cavity". In: (Submitted Apr. 2016) (cit. on pp. 19, 20, 24).

[22] M. Rachh, A. Klöckner, and M. O'Neil. "Fast algorithms for Quadrature by Expansion I: Globally valid expansions". In: *Journal of Computational Physics* 345 (Supplement C Sept. 15, 2017), pp. 706–731. ISSN: 0021-9991. DOI: 10.1016/j.jcp.2017.04.062. URL: http://www.sciencedirect.com/science/article/pii/S0021999117303418 (visited on 11/14/2017) (cit. on p. 37).

[23] M. Reis. *Fundamentals of magnetism*. First edition. Amsterdam: Academic Press, 2013. 264 pp. ISBN: 978-0-12-405545-2 (cit. on p. 4).

[24] S. A. Sauter and C. Schwab. *Boundary element methods*. Springer Series in Computational Mathematics 39. OCLC: 729934218. Berlin: Springer, 2011. 561 pp. ISBN: 978-3-540-68092-5 (cit. on pp. 9, 10, 13, 15–18, 23, 26).

[25] S. A. Wolf et al. "Spintronics: A Spin-Based Electronics Vision for the Future". In: *Science* 294.5546 (Nov. 16, 2001), pp. 1488–1495. ISSN: 0036-8075, 1095-9203. DOI: 10.1126/science.1065389. URL: http://science.sciencemag.org/content/294/5546/1488 (visited on 06/07/2017) (cit. on p. 1).

[26] Wolfram Research, Inc. *Mathematica*. Version 11.2. Champaign, Illinois, 2017 (cit. on p. 32).

[27] I. Žutić, J. Fabian, and S. Das Sarma. "Spintronics: Fundamentals and applications". In: *Reviews of Modern Physics* 76.2 (Apr. 23, 2004), pp. 323–410. DOI: 10.1103/RevModPhys.76.323. URL: https://link.aps.org/doi/10.1103/RevModPhys.76.323 (cit. on p. 1).

Appendix A. Fast Multipole Method

The fast multipole method (FMM) is a fast way to compute an approximation to either

$$u(\vec{\mathbf{x}}) = \int K(\vec{\mathbf{x}}, \vec{\mathbf{y}}) w(\vec{\mathbf{y}}) \, \mathrm{d}y \tag{A.1}$$

or

$$u(\vec{\mathbf{x}}) = \sum_{i=1}^{N} K(\vec{\mathbf{x}}, \vec{\mathbf{y}}_i) w_i. \tag{A.2}$$

The need for such a fast evaluation becomes clear if we want to compute the solution at N points $\vec{\mathbf{x}}_j$. Without an efficient scheme, the amount of operations needed lies in $\mathcal{O}(N^2)$. With the FMM the amount reduces to $\mathcal{O}(N \log N)$ or even $\mathcal{O}(N)$ operations [5]. In our case we want to apply the FMM to the transmission problem Eq. (3.9) which corresponds to an equation of the kind of Eq. (A.1). The following theorems are needed in order to apply the three dimensional FMM.

Theorem A.1 (Addition theorem for Legendre polynomials [5])**.** *Let P and Q be points with spherical coordinates (r, θ, φ) and (ρ, α, β), respectively, and let γ be the angle between them. Then*

$$P_\ell(\cos\gamma) = \sum_{m=-\ell}^{\ell} Y_\ell^{-m}(\alpha, \beta) Y_\ell^m(\theta, \varphi) \tag{A.3}$$

Here, the complex spherical harmonics Y are defined by the recursion

$$Y_\ell^m(\theta, \varphi) = \sqrt{\frac{(\ell - |m|)!}{(\ell + |m|)!}} P_\ell^{|m|}(\cos\theta) e^{im\varphi}. \tag{A.4}$$

Theorem A.2 (Multipole Expansion [5])**.** *The multipole expansion is a result of Theorems 4.3 and A.1. Suppose that k charges of strengths*

$$\{q_i, i = 1, \ldots, k\}$$

are located at the points

$$\{Q_i = (\rho_i, \alpha_i, \beta_i), i = 1, \ldots, k\},$$

with $|\rho_i| < a$. Then for any $P = (r, \theta, \varphi) \in \mathbb{R}^3$ with $r > a$, the potential $\phi(P)$ is given by

$$\phi(P) = \sum_{\ell=0}^{\infty} \sum_{m=-\ell}^{\ell} \frac{M_\ell^m}{r^{\ell+1}} Y_\ell^m(\theta, \varphi), \tag{A.5}$$

where

$$M_\ell^m = \sum_{i=1}^{k} q_i \rho_i^\ell Y_\ell^{-m}(\alpha_i, \beta_i). \tag{A.6}$$

Furthermore, for any $p \geq 1$,

$$\left|\phi(P) - \sum_{\ell=0}^{p} \sum_{m=-\ell}^{\ell} \frac{M_\ell^m}{r^{\ell+1}} Y_\ell^m(\theta,\varphi)\right| \leq \frac{A}{r-a}\left(\frac{a}{r}\right)^{p+1}, \tag{A.7}$$

where

$$A = \sum_{i=1}^{k} |q_i|. \tag{A.8}$$

Theorem A.3 (Translation of a multipole expansion [5])**.** *Suppose that l charges of strengths $q_1, q_2, \ldots, q_l$ are located inside the sphere D of radius a with center at $Q = (\rho, \alpha, \beta)$ and that for points $P = (r, \theta, \varphi)$ outside D, the potential due to these charges is given by the multipole expansion*

$$\Phi(P) = \sum_{\ell=0}^{\infty} \sum_{m=-\ell}^{\ell} \frac{O_\ell^m}{r'^{m+1}} Y_\ell^m(\theta', \varphi'), \tag{A.9}$$

where $P - Q = (r', \theta', \varphi')$. Then for any point $P = (r, \theta, \varphi)$ outside the sphere D_1 of radius $(a + \rho)$,

$$\Phi(P) = \sum_{j=0}^{\infty} \sum_{k=-j}^{j} \frac{M_j^k}{r^{j+1}} Y_j^k(\theta, \varphi), \tag{A.10}$$

where

$$M_j^k = \sum_{\ell=0}^{j} \sum_{m=-\ell}^{\ell} \frac{O_{j-\ell}^{k-m} i^{|k|-|m|-|k-m|} A_\ell^m A_{j-\ell}^{k-m} \rho^\ell Y_\ell^{-m}(\alpha, \beta)}{A_j^k} \tag{A.11}$$

with A_ℓ^m defined by

$$A_\ell^m = \frac{(-1)^\ell}{\sqrt{(\ell - m)!(\ell + m)!}}. \tag{A.12}$$

Furthermore, for any $p \geq 1$,

$$\left|\Phi(P) - \sum_{j=0}^{p} \sum_{k=-j}^{j} \frac{M_j^k}{r^{j+1}} Y_j^k(\theta, \varphi)\right| \leq \left(\frac{\sum_{i=1}^{l} |q_i|}{r - (a + \rho)}\right)\left(\frac{a + \rho}{r}\right)^{p+1}. \tag{A.13}$$

Theorem A.4 (Conversion of a multipole expansion into a local expansion [5])**.** *Suppose that l charges of strengths $q_1, q_2, \ldots, q_l$ are located inside the sphere D_Q of radius a with center at $Q = (\rho, \alpha, \beta)$, and that $\rho > (c + 1)a$ with $c > 1$. Then the corresponding translated multipole expansion Eq.* (A.9) *converges inside the sphere D_0 of radius a centered at the origin. Inside D_0, the potential due to the charges q_i is described by a local expansion*

$$\Phi(P) = \sum_{j=0}^{\infty} \sum_{k=j}^{j} L_j^k Y_j^k(\theta, \varphi) r^j, \tag{A.14}$$

where

$$L_j^k = \sum_{\ell=0}^{\infty} \sum_{m=-\ell}^{\ell} \frac{O_\ell^m i^{|k-m|-|k|-|m|} A_\ell^m A_j^k Y_{j+\ell}^{m-k}(\alpha,\beta)}{(-1)^\ell A_{j+\ell}^{m-k} \rho^{j+\ell+1}}, \tag{A.15}$$

with A_r^s *defined by Eq.* (A.12)*. Furthermore, for any* $p \geq 1$*,*

$$\left| \Phi(P) - \sum_{j=0}^{p} \sum_{k=-j}^{j} L_j^k Y_j^k(\theta,\varphi) r^{j+1} \right| \leq \left(\frac{\sum_{i=1}^{l} |q_i|}{ca-a} \right) \left(\frac{1}{c} \right)^{p+1} \tag{A.16}$$

Theorem A.5 (Translation of a local expansion [5])**.** *Let* $Q = (\rho, \alpha, \beta)$ *be the origin of a local expansion*

$$\Phi(P) = \sum_{\ell=0}^{p} \sum_{m=-\ell}^{\ell} O_\ell^m Y_\ell^m(\theta',\varphi') r'^\ell, \tag{A.17}$$

where $P = (r, \theta, \varphi)$ *and* $P - Q = (r', \theta', \varphi')$*. Then*

$$\Phi(P) = \sum_{j=0}^{p} \sum_{k=-j}^{j} L_j^k Y_j^k(\theta,\varphi) r^j, \tag{A.18}$$

where

$$L_j^k = \sum_{\ell=j}^{p} \sum_{m=-\ell}^{\ell} \frac{O_\ell^m i^{|m|-|m-k|-|k|} A_{\ell-j}^{m-k} A_j^k Y_{\ell-j}^{m-k}(\alpha,\beta) \rho^{\ell-j}}{(-1)^{\ell+j} A_\ell^m}, \tag{A.19}$$

with A_r^s *defined by Eq.* (A.12)*.*

Additionally, the definition of the following terms is used throughout the description of the FMM.

Definition A.1 (Nearest neighbors [5])**.** *Two boxes are said to be* near neighbors *if they are at the same refinement level and share a boundary point. (A box is a near neighbor of itself.)*

Definition A.2 (Well separated [5])**.** *Two boxes are said to be* well separated *if they are at the same refinement level and are not near neighbors.*

Definition A.3 (Interaction list [5])**.** *With each box* i *is associated an* interaction list*, consisting of the children of the near neighbors of* i*'s parent which are well separated from box* i*.*

The algorithm consists of two basic ideas: (1) use the multipole expansion Theorem A.2 to compute interactions between well separated boxes for each box in the finest refinement level, (2) compute multipole expansion for parent boxes without reconsidering particles using Theorem A.3, (3) compute a local expansion (see Theorem A.4) of each box to account for interactions with well separated boxes (starting from level $l = 2$ downwards), (4) add these contribution to the box's children using Theorem A.5, (5) and compute interactions with particles in the interaction list directly. Now, the algorithm is described in more detail.

Let the computational domain be a cube. The refinement level of said cube is denoted by $l = 0$.

(1) Initialization
   (a) Choose the level of refinement $n \approx \log_8 N$, s.t. a box in the highest level of refinement $l = n$ consists of approximately s particles
   (b) Choose precision ϵ
   (c) Subdivide the cube into 8 cubes, called children (level $l+1$)
   (d) Subdivide each children until level $l = n$, recursively

(2) Upward pass
   (a) Compute multipole expansion (see Theorem A.2) at grid level $l = n$ truncating at $p \approx -\log_2 \epsilon$
   (b) Go to the next coarser level, shift center of child's box expansion to current boxes center (see Theorem A.3) and add them together
   (c) Repeat Item 2b until level $n = 0$

(3) Downward pass
   (a) Convert multipole expansion of current level box's interaction list into local expansion using Lemma 2.4 of Greengard and Rokhlin [10] and add them to $\Psi_{l,\text{ibox}}$
   (b) Form $\Psi_{l+1,\text{ibox}}$ using Lemma 2.5 of Greengard and Rokhlin [10]
   (c) Repeat Item 3a until level $l = n - 1$
   (d) Compute interactions at level $l = n$
   (e) Evaluate local expansions at particle positions to form $\phi_{n,\text{ibox}}(\vec{\mathbf{x}}_j)$
   (f) Compute potential due to nearest neighbors of box at level $l = n$
   (g) Add direct and far fields for every particle in box at level $l = n$

Appendix B. Code Listings

```
R = 0.5;
zs = (0.01:0.01:4)';
points = [zs zs zs];
% Exact solution.
[~, ~, r] = Cart_To_Sph(points);
int = r <= R;
ext = ~int;
Phi = zeros(size(zs));
Phi(int) = -2/9*zs(int) + 2/3*zs(int).*log(r(int)/R);
Phi(ext) = -2*R^3/9 * zs(ext)./(r(ext).^3);
% Approximate solution.
Geom = Geom_AddSphere([0 0 0], R);
% rhs
M = @(theta, phi, r) [sin(theta) ...
                      cos(theta) ...
                      zeros(size(r))];
f = @(theta, phi, r) 2*cos(theta)./r;
g = @(theta, phi, r) zeros(size(r));
% Discretization settings.
axis_sym = 0;
eta = 1;
tol = 1e-9;
% Default shift.
shift = 'sym';
% Default solver.
solver.type = 'diis';
solver.Q = 5;
calc_derivative = true;
% Radius discretization.
rN = 60;
% SH truncation.
lmax = 10;
% Lebedev Quadrature orders.
GORDER = [3,5,7,9,11,13,15,17,19,21,23,25,27,29,31,35,41,47,53,...
    59,65,71,77,83,89,95,101,107,113,119,125,131];
```

Listing 1. Exact Solution and Set-Up for Section 5.3.

```
1.7438 -0.352006 -1.22404 0.218589
1.97826 0.878527 -0.012792 0.24989
3.68916 -0.467149 0.860277 0.237595
4.10904 0.164432 -0.00898384 0.247295
5.03393 1.00227 0.734712 0.104963
5.84536 1.16304 0.362377 0.184054
7.06519 -0.678599 0.52311 0.208328
7.61125 1.34871 -0.222961 0.249963
8.85138 1.03927 1.62336 0.187603
10.1095 -0.90469 -0.283181 0.200881
```

Listing 2. Data for the Creation of Spheres. From left to right a line contains the (x, y, z) coordinates and the radius r. The file is created, such that the spheres don't overlap.